PHOTOGRAPH THIS SHEET

AD-A207 062

DTIC ACCESSION NUMBER

DTIC FILE COPY

LEVEL

1

INVENTORY

DNA-TR 86-51-V2

DOCUMENT IDENTIFICATION

31 MAY 1986

This document has been approved for public release and sale; its distribution is unlimited.

DISTRIBUTION STATEMENT

ACCESSION FOR	
NTIS GRA&I	☒
DTIC TAB	☐
UNANNOUNCED	☐
JUSTIFICATION	
BY	
DISTRIBUTION /	
AVAILABILITY CODES	
DIST	AVAIL AND/OR SPECIAL
A-1	

DISTRIBUTION STAMP

DTIC
ELECTE
APR 24 1989
S D

DATE ACCESSIONED

DATE RETURNED

089 4 21 088

DATE RECEIVED IN DTIC

REGISTERED OR CERTIFIED NO.

PHOTOGRAPH THIS SHEET AND RETURN TO DTIC-FDAC

DTIC FORM 70A MAR 86

DOCUMENT PROCESSING SHEET

PREVIOUS EDITION MAY BE USED UNTIL STOCK IS EXHAUSTED.

DNA-TR-86-51-V2

ASSESSMENT OF THE VULNERABILITY AND LETHALITY OF AEROSPACE SYSTEMS

Volume II—Laser Coupling Measurements

Bayard S. Holmes
SRI International
333 Ravenswood Avenue
Menlo Park, CA 94025-3493

31 May 1986

Technical Report

CONTRACT No. DNA 001-82-C-0267

Approved for public release;
distribution is unlimited.

THIS WORK WAS SPONSORED BY THE DEFENSE NUCLEAR AGENCY
UNDER RDT&E RMSS CODE B346085764 X99QMXXC00004 H2590D.

Prepared for
Director
DEFENSE NUCLEAR AGENCY
Washington, DC 20305-1000

Destroy this report when it is no longer needed. Do not return to sender.

PLEASE NOTIFY THE DEFENSE NUCLEAR AGENCY ATTN: TITL, WASHINGTON, DC 20305 1000, IF YOUR ADDRESS IS INCORRECT, IF YOU WISH IT DELETED FROM THE DISTRIBUTION LIST, OR IF THE ADDRESSEE IS NO LONGER EMPLOYED BY YOUR ORGANIZATION.

REPORT DOCUMENTATION PAGE

1a. REPORT SECURITY CLASSIFICATION UNCLASSIFIED	1b. RESTRICTIVE MARKINGS
2a. SECURITY CLASSIFICATION AUTHORITY N/A since Unclassified	3 DISTRIBUTION/AVAILABILITY OF REPORT Approved for public release; distribution is unlimited.
2b. DECLASSIFICATION/DOWNGRADING SCHEDULE N/A since Unclassified	
4 PERFORMING ORGANIZATION REPORT NUMBER(S) SRI PYU 4539	5. MONITORING ORGANIZATION REPORT NUMBER(S) DNA-TR-86-51-V2
6a. NAME OF PERFORMING ORGANIZATION SRI International 6b. OFFICE SYMBOL (If applicable)	7a. NAME OF MONITORING ORGANIZATION Director Defense Nuclear Agency
6c. ADDRESS (City, State, and ZIP Code) 333 Ravenswood Avenue Menlo Park, CA 94025-3493	7b. ADDRESS (City, State, and ZIP Code) Washington, DC 20305-1000
8a. NAME OF FUNDING/SPONSORING ORGANIZATION 8b OFFICE SYMBOL (If applicable) SPAS/Wolf	9. PROCUREMENT INSTRUMENT IDENTIFICATION NUMBER DNA 001-82-C-0267
8c. ADDRESS (City, State, and ZIP Code)	10. SOURCE OF FUNDING NUMBERS PROGRAM ELEMENT NO. 62715H; PROJECT NO X990MXX; TASK NO C; WORK UNIT ACCESSION NO DH007240

11 TITLE (Include Security Classification)
ASSESSMENT OF THE VULNERABILITY AND LETHALITY OF AEROSPACE SYSTEMS
Volume II—Laser Coupling Measurements

12 PERSONAL AUTHOR(S)
Holmes, Bavard S.

13a TYPE OF REPORT	13b TIME COVERED	14. DATE OF REPORT (Year, Month, Day)	15 PAGE COUNT
Technical	FROM 840901 TO 860415	860531	60

16. SUPPLEMENTARY NOTATION
This work was sponsored by the Defense Nuclear Agency under RDT&E RMSS Code B346085764 X990MXXC00004 H2590D.

17 COSATI CODES			18 SUBJECT TERMS (Continue on reverse if necessary and identify by block number)
FIELD	GROUP	SUB-GROUP	Laser Coupling Wave Propagation Stress Gages
20	09		
20	11		

19 ABSTRACT (Continue on reverse if necessary and identify by block number)

Piezoresistant gages were used to measure the surface pressure histories produced by pulsed lasers on targets either in air or in a vacuum. A new vapor-deposited ytterbium gage was developed for these measurements. This gage has improved temporal response over older ytterbium gage designs. Calculations relating surface pressure to gage resistance change showed that pressure rise times of about 10 ns can be measured with this gage. In addition to the surface pressure measurements, total impulse was measured during the experiment series in air.

The pressure and impulse measurements in air were made using neodymium-glass laser (1.06 -μm wavelength) with a pulse width of 30 ns, pulse energies from 100 to 1000 J, and spot sizes of 1 and 2 cm diameter. The pressure measurements in a vacuum were made using an XeF laser (3.532 -μm wavelength) with a pulse width of 1.5 μs, pulse energies from 168 to 241 J, and spot sizes of 8 and 12.4 mm diameter.

20 DISTRIBUTION/AVAILABILITY OF ABSTRACT	21 ABSTRACT SECURITY CLASSIFICATION	
☐ UNCLASSIFIED/UNLIMITED ☒ SAME AS RPT ☐ DTIC USERS	UNCLASSIFIED	
22a NAME OF RESPONSIBLE INDIVIDUAL Sandra E. Young	22b TELEPHONE (Include Area Code) (202) 325-7042	22c. OFFICE SYMBOL DNA/CSTI

DD FORM 1473, 84 MAR 83 APR edition may be used until exhausted. All other editions are obsolete.

19. ABSTRACT (Continued)

This report supplements two other volumes: Volume I - Analysis of MIDAS MYTH Lethality Experiments, and Volume III - Structural Response of Liquid-Fueled Boosters.

SUMMARY

A new piezoresistant gage technique was developed for use in measuring the stress histories produced in solid targets by a pulsed laser. This technique uses vapor-deposited ytterbium gages encapsulated in a gage package designed to record very fast-rising pulses. The package was designed through a series of one-dimensional calculations that indicate that pulse rise times of about 10 ns can be measured. In addition, two-dimensional calculations indicate a low gage sensitivity to the two-dimensional effects introduced into a target by the finite laser spot size.

In addition to the stress gage package, a pendulum was developed to measure the impulse produced by pulsed lasers. This device used a beam to support the pendulum (see Figure 8), allowing precise positioning, and an optical scanner to measure pendulum motion. The use of the optical scanner allowed the measurement of the pendulum velocity over short distances (about 0.2 mm) so that the impulse could be measured without the effects introduced by large pendulum displacements and long measurement periods.

Two series of pressure measurements were made with the gage package to determine the coupling of pulsed lasers of near visible wavelength (primarily to aluminum targets): one series was performed in air and the other in a vacuum. In the first series of experiments, a neodymium-glass (1.06 -μm-wavelength) laser was used with a nominal pulse duration of 30 ns and spot sizes of 1 and 2 cm diameter. In this experiment series, the targets were in air at near standard atmospheric conditions and the coupling was primarily through air plasmas that were ignited on the target surface. In some of the experiments the impulse was measured using the pendulum.

Fourteen pressure histories were obtained in the in-air coupling experiments. Peak pressures measured in these experiments were consistently lower than those measured in previous experiments, albeit under different conditions. These lower peak pressures are apparently due to the formation of "superdetonation" waves instead of the normal laser supported detonation (LSD) waves. This conclusion is further supported by plasma velocity measurements that show higher velocities than LSD wave velocities.

The impulse was measured during the in-air coupling experiments using pendulums of different diameters. Total impulse data from these experiments are consistent

with the integral of the pressure-time history data but indicate that about 40% of the impulse measured by the pendulum may be due to late-time effects. This late-time impulse occurs too late to affect structural response. Thus, using the impulse data obtained from pendulum measurements will tend to overestimate target response. We recommend that impulse data be supplemented by pressure-time histories whenever possible.

The second series of pressure measurements was performed in a vacuum using an XeF laser of approximately 3.5 μm wavelength with a nominal pulse duration of 1.5 μs and spot sizes of 8 mm and 12.4 mm diameter. Seven pressure-time histories were obtained in this experiment series.

Pressure-time histories measured in the in-vacuum coupling experiments showed the characteristics of coupling through direct target vaporization. The pressure-time histories had the shape of the laser pulse with a rapid pressure decay after the laser pulse was completed. Plots of peak pressure as a function of flux and impulse intensity as a function of pulse energy showed a great deal of scatter in these experiments. However, both peak pressure and impulse intensity increased rapidly with increasing laser pulse flux and energy indicating a strong sensitivity to these parameters over their range in these experiments. Coupling coefficients measured in these experiments ranged from 0.25 to 1.5 dyne-s/J.

PREFACE

This work was sponsored by the Defense Nuclear Agency under Contract DNA 001-82-C-0167. Major Charles Martin was the contract technical monitor. Major Martin's technical advice and continued support are gratefully acknowledged. In addition, this work would not have been possible without the facilities and support of the Battelle Columbus Laboratories and Dr. Craig Walters and the facilities and support of Avco Everett Research Laboratory and Dr. Carolyn Duzy and their respective staffs who spent many hours setting up instrumentation, providing laser diagnostics and advice, and performing the many other tasks associated with experimental stress measurements. At SRI International, Darwin Henley built the gage packages and Dan Walter fielded the electronics. They provided the basic ingredients that made the stress measurements possible.

TABLE OF CONTENTS

LIST OF ILLUSTRATIONS

LIST OF TABLES

SECTION 1

INTRODUCTION

A key problem in the assessment of pulsed laser weapon effectiveness is the determination of the surface pressure loads produced on the target by the laser. Both impulse intensity and peak pressure affect target damage. In addition, scaling small-scale laboratory experiments to full-scale scenarios requires a good understanding of the coupling phenomena. The measurements reported here were performed to better define the mechanical coupling parameters of pulsed lasers and, in particular, the history of surface pressure produced by laser-target interaction.

Two sets of experiments were performed in laser facilities at Battelle Memorial Institute in Columbus, Ohio, and at Avco Everett Research Laboratory in Everett, Massachusetts. The objective of the Battelle experiments was to determine the pressure-time history for target interactions in air when coupling is through an air plasma or laser-supported detonation (LSD). A further objective of the Battelle experiments was to refine our understanding of this interaction process at late times as the pressure in the laser plasma decays. This experiment series also included direct measurement of impulse. The objective of the Avco experiments was to measure pressure-time histories produced when the target is in a vacuum.

In the following sections we first describe the design of the piezoresistant gages used in the pressure measurements. In discussing the gage package design, we examine the requirements placed on the pressure measurement by the need to predict structural response. Section 3 describes the experiments and results of the in-air laser coupling experiments (Battelle experiment series), and Section 4 describes the in-vacuum laser coupling experiments and results (AVCO experiment series).

SECTION 2

GAGE PACKAGE DESIGN

2.1 MEASUREMENT REQUIREMENTS.

The characteristics of the surface pressure history produced by a pulse laser depend on the laser pulse shape and spot size and whether the target is in air or in a vacuum. For interactions in air in which the laser flux is sufficient to ignite an air plasma, the surface pressure is usually characterized by a step increase in pressure followed by an exponential decay as the air plasma decays. The rise time of the pressure pulse is potentially on the order of the time required for the breakdown process to occur (perhaps 100 ns)[1]. Thus, the temporal resolution of the gage should be on the same order or better, if possible. In practice, however, the spatial variation in plasma formation becomes important, and actual pressure rise times measured over a large area may appear much longer because of spatial variations in pressure.

The decay process for laser target interaction in air can last many laser pulse durations, so the total impulse on the target may be produced over a long period of time. However, the impulse delivered within the target's response time (that is, the prompt impulse) determines structural response. The time window of interest for laboratory-scale experiments can be estimated by scaling the response of full-scale targets and using the scaling laws for structures.[2] For example, for large aerospace structures with a diameter of about 3 m, the structural response modes of pulse buckling or denting are completed in less than 10 ms. Assuming a full-scale laser spot diameter of 1.5 m and a laboratory-scale spot size of 1 cm, the laboratory experiment is 1/1500 scale. In these experiments, time scales as the scale factor[2], so the characteristic structural response time for the laboratory experiment is

$$10 \text{ ms}/1500 = 7 \text{ } \mu\text{s}$$

In a laboratory-scale experiment with a pressure history characterized by an exponential decay, the pressure at times after 7 μs would have no further effect on structural response and need not be measured accurately to estimate target damage. In the pressure measurements reported in Section 3, we usually measured pressure over time windows of 10 μs . We also independently measured total impulse during

the in-air coupling experiments for comparison with the prompt impulse measured by the gage package.

The measurement requirements for the in-vacuum experiments are similar to those for the in-air experiments. However, the surface pressure decays rapidly after termination of the laser pulse and the time window of interest is approximately equal to the laser pulse duration. In the experiments reported in Section IV, the recording time of the gage package was about three times the laser pulse duration.

Vapor-deposited ytterbium piezoresistant gages were used in all the experiments. This gage technique is based on the change in resistivity of ytterbium with stress although changes in gage shape (strain) also change the gage resistance. The gages were imbedded in the laser target rather than placed on the surface to protect the gages from the laser plasma. Thus, they sense the stress in the target rather than surface pressure. In order to highlight this distinction, all records reported here give stress as the ordinate rather than pressure. Design of the laser target or "gage package" determines the relationship between surface pressure and gage response and it will be shown that the stress component normal to the gage in our present design is nearly identical to the surface pressure above the gage. We therefore extract peak surface pressures and impulse intensities from the stress records directly without further correction.

2.2 UNIAXIAL-STRAIN GAGE PACKAGE RESPONSE.

The gage packages used in these experiments were constructed in layers to facilitate gage placement under the target surface. The first layer (cover plate) of the target was usually aluminum (the target material in the experiments). Subsequent layers were an electrically insulating material that protected the gage and a backing plate. Three gage package designs were examined to determine which arrangement of target plate, gage insulating layer, and backing plate produced the best gage temporal response. The candidate designs are shown in cross section in Figure 1. Figure 1(a) shows a gage package made with a gage backing plate with a mechanical impedance* lower than that of aluminum and encapsulated carbon gages (low-impedance package).

*Mechanical impedance is the product of sound speed and density.

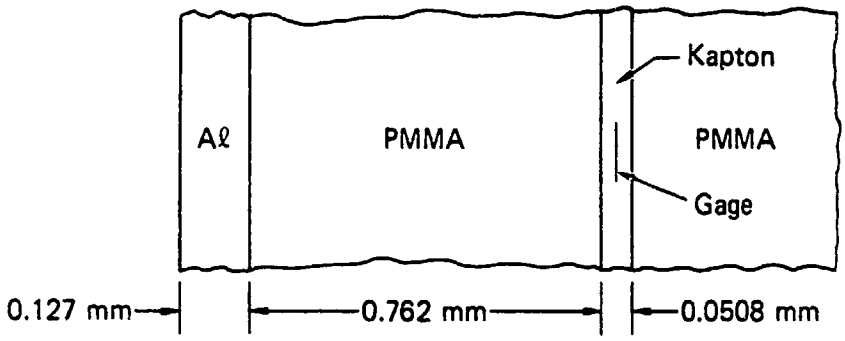

(a) Low impedance package with encapsulated carbon gages

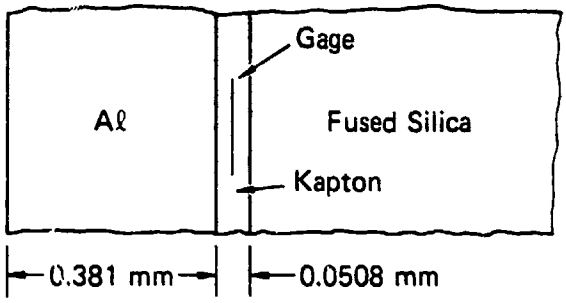

(b) High impedance package with encapsulated carbon gages

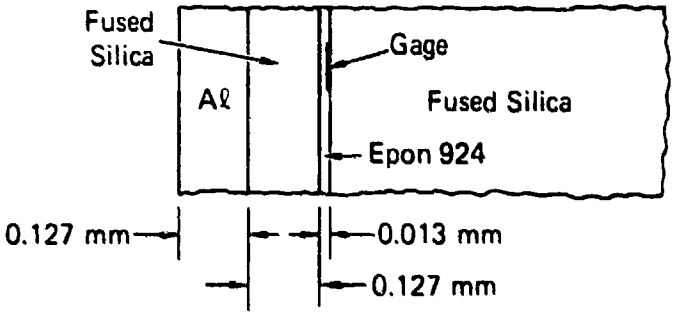

(c) High impedance package with direct-deposited ytterbium gages

JA-4539-12A

Figure 1. Cross sections of alternative gage package designs.

Figures 1(b) and 1(c) show gage packages made with backing plates with a mechanical impedance nearly equal to that of aluminum. The package in Figure 1(b) uses encapsulated carbon gages that provide a thick low-impedance gage insulating layer, and the package shown in Figure 1(c) uses direct-deposited gages that provide a very thin gage insulating layer. In the low-impedance carbon gaged package [Figure 1(a)], the gage is encapsulated in Kapton in a PMMA substrate and placed under the aluminum cover plate. Because PMMA has a much lower mechanical impedance than aluminum, the interface between the aluminum and PMMA layers changes the magnitude of waves transmitted from the surface to the gage layer (right-traveling waves) and also generates reflected waves that travel back to the target surface (left-traveling waves). A series of reflections between the surface and the gage plane is required to equilibrate the stress at the surface and the gage plane. In the high-impedance carbon gage package [Figure 1(b)], the gage is again encapsulated in Kapton, but the Kapton layer is placed directly between the aluminum cover plate and a fused-silica backing place. The aluminum and fused silica have similar impedances in contrast to the low-impedance Kapton; thus, a significant impedance mismatch results at the interfaces at the gage insulating layer. Several wave reflections in the insulating layer are required to bring it to the same stress as the surrounding material. Note that these first two gage package designs can be made with either commercially available encapsulated carbon gages or specially fabricated vapor-deposited ytterbium gages.

In the third gage package, ytterbium gages are vapor-deposited directly onto a fused-silica backing plate, and a fused-silica insulator is bonded directly over the gages using a very thin epoxy layer [Figure 1(c)]. In this design, the gage layer (Epon 924 epoxy) again has a low impedance, but the effect of the impedance mismatch is minimized because the epoxy Layer is very thin.

The response of the gage packages in uniaxial strain was estimated using the SRIPUFF8 computer code. For the calculation, an idealized surface pressure history was chosen to represent the laser generated pulse. The response to this input pulse was calculated for each gage package with SRIPUFF8 for uniaxial strain. Table 1 lists the material properties used in the calculations. Figure 2 shows the calculated stress at the gage plane for each gage design as well as the input pulse used

Table 1. Material properties used in calculations of response of different gage packages.

Material	Bulk Modulus (MPa)	Shear Modulus (MPa)	Density (g/cm)
6061-T6 Aluminum	6.67×10^4	2.67×10^4	2.7
Fused silica	3.665×10^4	3.10×10^4	2.2
Kapton/epoxy	8.43×10^3	3.0×10^3	1.2
PMMA	6.68×10^3	1.07×10^3	1.18

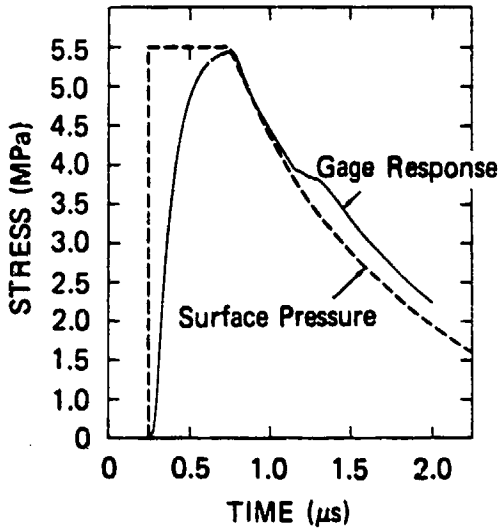

(a) Low impedance package with encapsulated gages

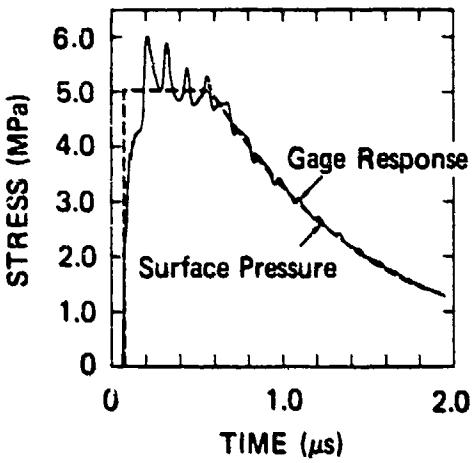

(b) High impedance package with encapsulated gages

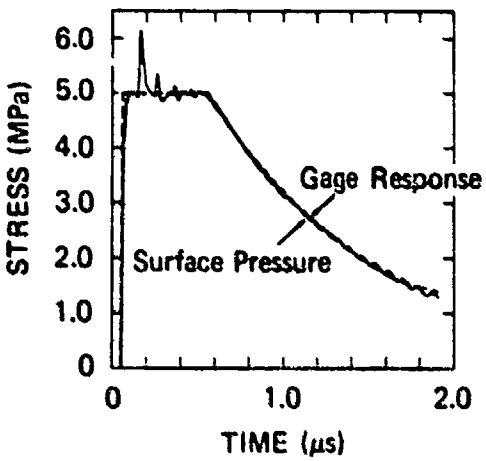

(c) High impedance package with direct-deposited gages

JA-4539-64

Figure 2. Calculated gage package response in uniaxial strain.

in the calculation. For easier comparison, the input surface pressure has been offset in time by the transit time from the surface to the gage.

Figure 2 shows the influence of impedance mismatches in the gage package. The low-impedance gage package is sluggish at early times and overresponds at late times because the aluminum layer acts with the PMMA backing plate as a mass-spring system. However, because the layers under the aluminum plate have a nearly uniform impedance, there are no high-frequency oscillations in stress at the gage plane.

In response to the same input surface pressure history, the high-impedance package with the thick low-impedance gage plane [Figure 2(b)] exhibits a distinct oscillation in response to the rapid rise in surface pressure at the beginning of the pressure pulse. This is caused by wave reflections that originate in the low-impedance insulating layers.

The high-impedance package with the thin gage insulating layer [Figure 2(c)] follows the surface pressure more closely. The stress at the gage plane shows some oscillations because of the low-impedance gage layer, but these are of shorter duration and less amplitude than those for the high-impedance package. In practice, these short spikes are usually attenuated by the spatial averaging of the gage and by dispersion.

Because a very fast gage response was required for the experiments, we chose the third gage package design and used direct-deposited gages on a fused silica backing plate. The gages were prepared by vapor depositing ytterbium through a mask. Figure 3 shows three of the gages before the aluminum cover plate was attached.

Two gage grid designs were used in the current experiments. The first grid design was 8 mm square and is shown in Figure 3. The 12 legs of the grid are 0.3 mm wide by 8 mm long. This design was used only for gage development. The second grid design was 3.9 mm by 3.3 mm overall with five legs 0.3 mm wide by 3.9 mm long. This design was used in all the experiments. Gages of both types were made with a nominal gage resistance of 50 ohm by varying the ytterbium thickness. The nominal thickness of the ytterbium was 300/nm for the 3.9 mm x 3.3 mm gages.

2. 3 TWO-DIMENSIONAL GAGE PACKAGE RESPONSE.

Impedance variations in the layers of the gage package give rise to errors in gage response in uniaxial strain. A second source of error arises from the spatial variation in pressure on the gage package surface due to the finite size of the

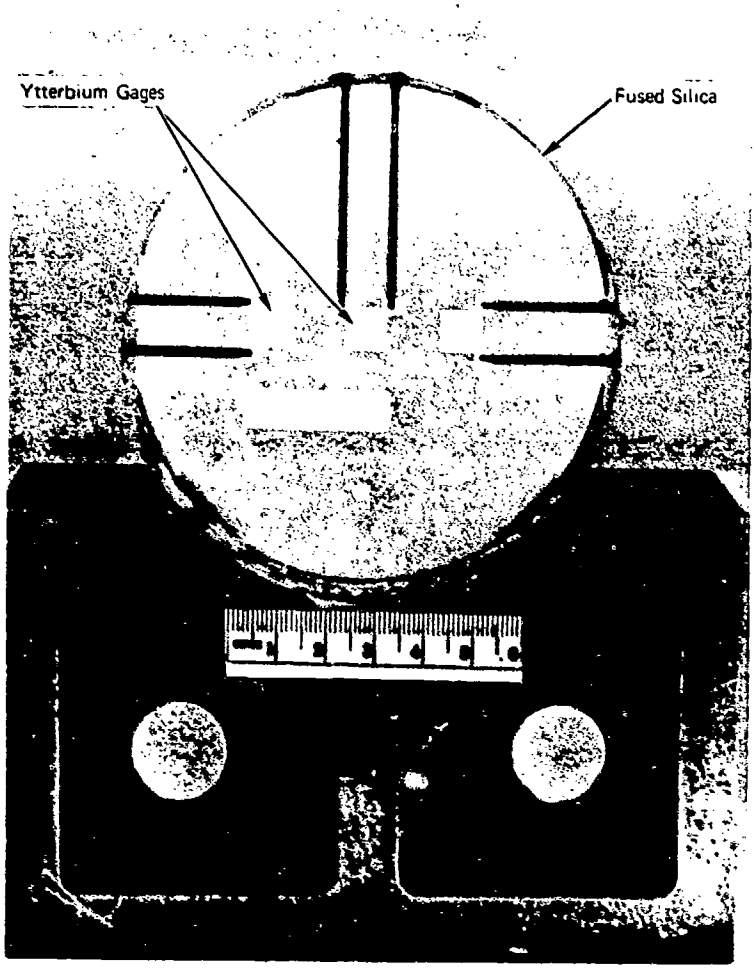

JP-4539-65A

Figure 3. Vapor-deposited ytterbium gages on fused-silica backing plate.

laser spot. As the gage package responds, these spatial variations in surface pressure cause a departure from the uniaxial strain state. Because the piezoresistant gages may respond to the additional components of stress and strain, large errors in gage response can result.

To estimate the importance of this effect, we analyzed the response of the gage package using the TROTT two-dimensional finite difference code. For the low stresses in the experiments, plastic deformation of the gage and surrounding material does not occur and response is linear and elastic. The calculation was performed on a loaded half-space assuming azimuthal symmetry and using a surface loading approximating that produced by a pulsed laser. The spatial and temporal variation of the loading is given in Figure 4. Also indicated in the figure is the two-dimensional nature of the gage displacements and strains.

Figure 5 shows the strain history predicted in the two-dimensional calculations. In Figure 5(a) the predicted axial strain (solid line) is compared with the surface pressure divided by the axial compressibility (dotted line). As expected, the two curves are similar at early times, but deviate at times greater than 3 μs because of edge effects. The arrival of waves from the edge of the laser spot is also evident in the radial strain, Figure 5(b), whereas shear strains remain small at all times, Figure 5(c).

The effect of the deviation from uniaxial strain was estimated by measuring the gage package sensitivity to normal strains (the shear strains were assumed negligible). Because the gage response is linear and elastic, the resistance change of the gage is uniquely determined by the local state of strain in the gage package. Therefore

$$\Delta R/R = K_{ij} e_{ij} \qquad (1)$$

where R is gage resistance, e_{ij} are the strain components, and K_{ij} are constants to be determined. The planes indicted by the strain state are aligned with the gage package as shown in Figure 6.

Neglecting shear strains, the only significant coefficients are K_{11}, K_{22}, and K_{33}. These coefficients were measured in static tests in which sample gages were subjected to hydrostatic loading and uniaxial strain in the gage plane (directions 1 and 2). The results of the measurements are as follows:

$$K_{11} = -3.4 \qquad K_{22} = -5.2 \qquad K_{33} = -27.7$$

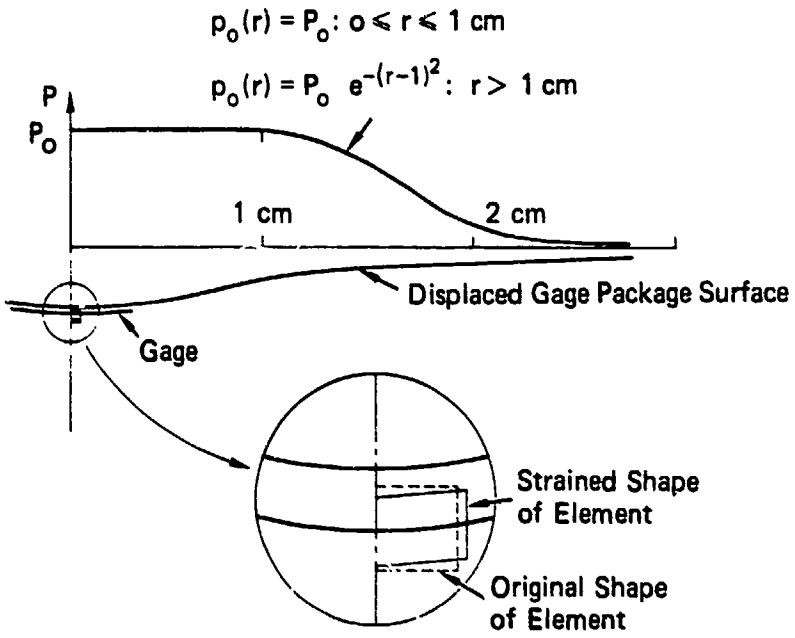

(a) Spatial Distribution of Pressure and Gage Package Deformation

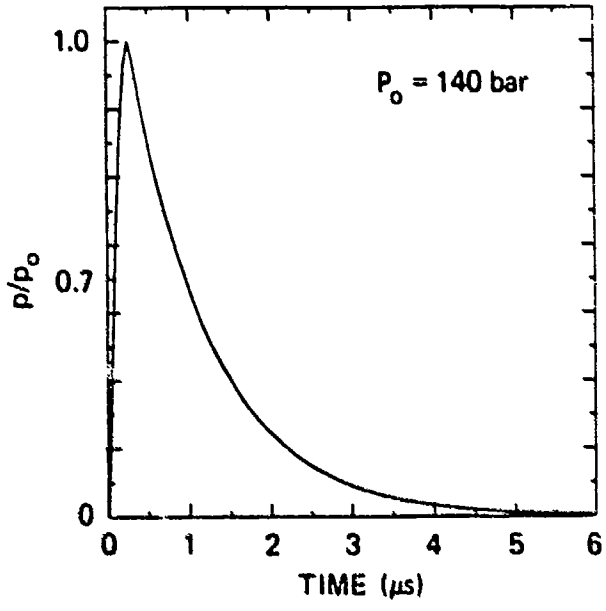

(b) Relative Pressure History at any Location

JA-4539-66A

Figure 4. Surface load used in two-dimensional response calculation.

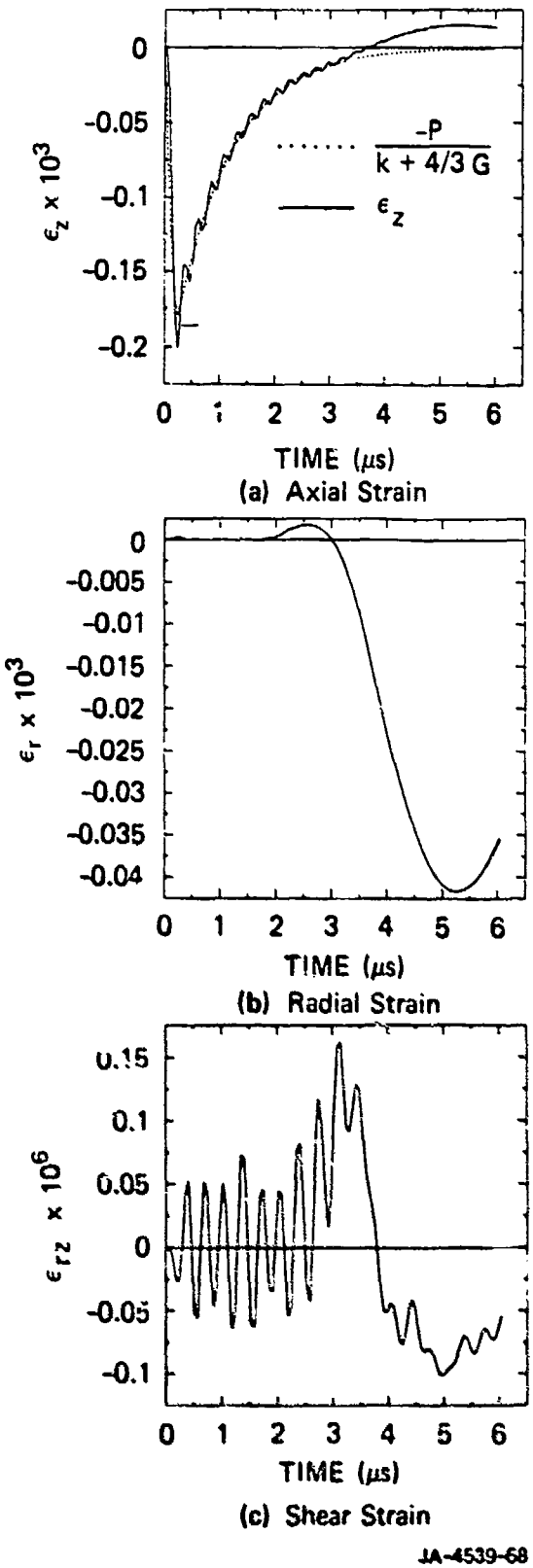

Figure 5. Calculated state of strain at target center.

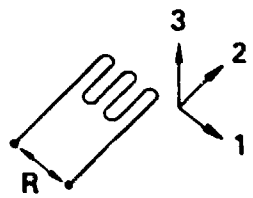

JA-4537-126

Figure 6. Gage orientation for equation (1).

Substituting these values into Fquation (1) and using the strains shown at 5 μs in Figure 5 give a change in resistance corresponding to a stress of -0.6 MPa in uniaxial strain, whereas the actual surface pressure at this time was about +0.2 MPa. Thus, we expect that at late times gage measurements will be in error by about -0.8 MPa.

2.4 GAGE PACKAGE CONSTRUCTION.

In the tests, one gage package configuration was used for the in-air experiments and another for the in-vacuum experiments. For the in-air experiments, three gages were embedded in 100-mm-diameter fused-silica blanks. These blanks were constructed by first depositing the gages on the blanks shown in Figure 3. A 1-mm-thick plate of fused silica was bonded over the gages and then ground to a thickness of 0.075 mm. An aluminum cover disk was then attached to the gage package for each shot by covering the package with grease and then rolling on the cover disk with a small plastic roller. By measuring the thickness of the gage package before and after adding the cover disk, we estimated the thickness of the grease layer to be less than 0.005 mm. This very thin layer of grease did not affect the pressure history noticably.

In the in-vacuum experiments, we were concerned that the use of an oil or grease layer would not guarantee that the aluminum cover disk would stay on the gage package as the test chamber was evacuated. To avoid using the grease layer, we developed a second gage package design in which the aluminum cover disk was bonded to the fused silica with epoxy. Because this gage package could be used only for one shot, the gage package diameter was reduced to 38 mm and only one or two gages were built into each package. This second gage package design was used in all the in-vacuum experiments.

A special power supply that could be incorporated into the gage package was built for these experiments. In an effort to minimize the electrical interference from the laser, the power supply was battery powered. This arrangement eliminated dependence on exterior power which is often subject to noise, and also provided integral shielding. Figure 7 is a photograph of the power supply/gage package showing the replaceable gage package (target) section.

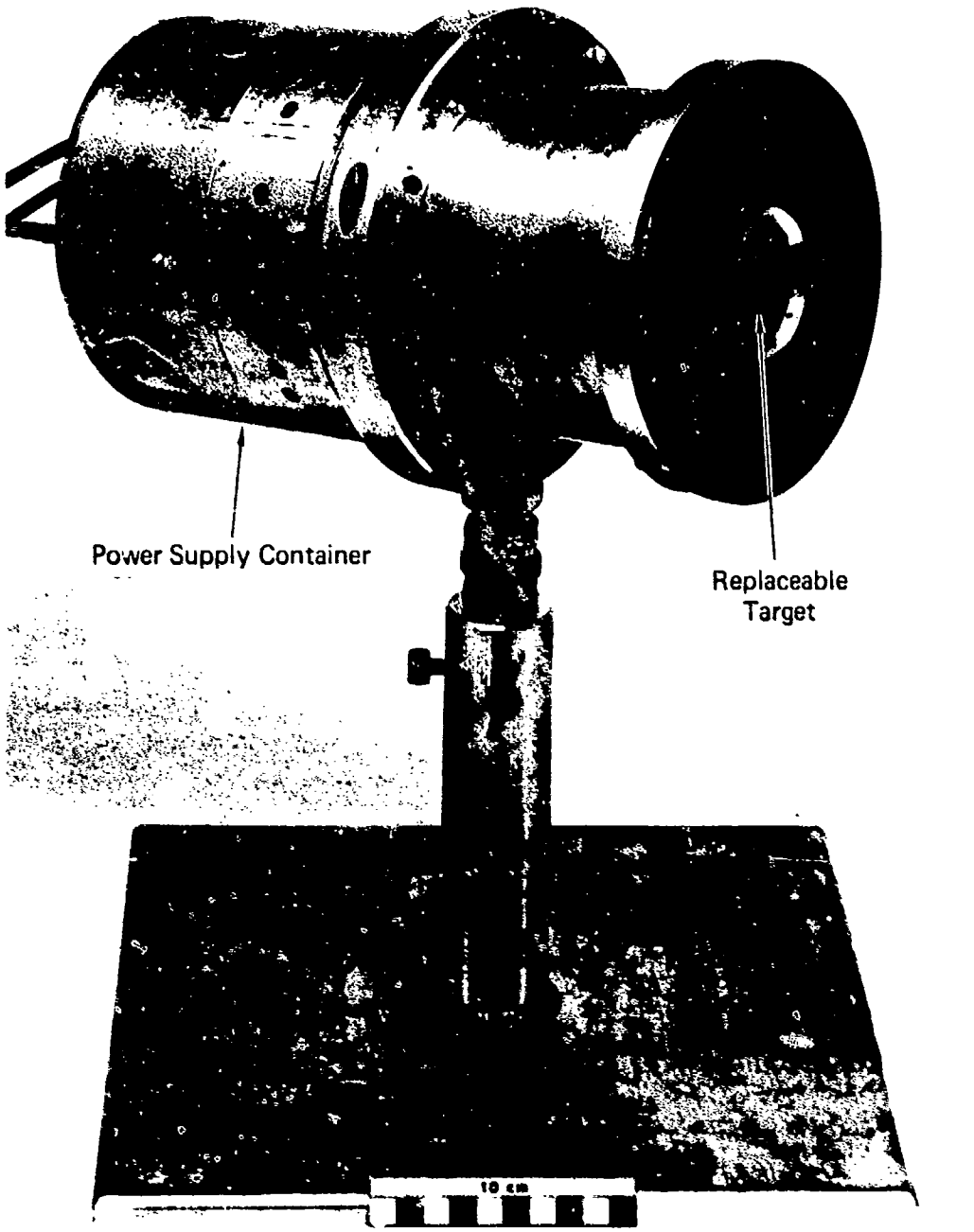

Figure 7. Gage package with integral power supply.

2.5 IMPULSE MEASUREMENTS.

Total impulse was measured directly in some of the in-air experiments using the instrument shown in Figure 8. In this measurement, a heavy mass (pendulum bob) is mounted on a thin titanium beam. The mass of the beam is small compared with that of the pendulum bob (the correction for the beam mass is included in the pendulum calculation). The use of the beam to support the pendulum allows for precise alignment of the pendulum in the target plate, which minimizes leakage of the plasma past the pendulum. A radial clearance of 0.05 mm was maintained in all experiments. The displacement history of the pendulum is measured with a fiber optic scanner, which transmits light to the back of the pendulum and then intercepts the reflected light. The scanner was mounted onto a micrometer head for calibration. The error in the total measurement of the momentum of the pendulum with this system is estimated to be less than ±5%.

Pendulum diameters were varied as was spot size in the experiments so that the impulse contributions from inside and outside the laser spot could be estimated. Pendulum diameters of 1, 2, 3, and 6 cm were used in the Battelle experiments. Laser spot diameters were 1 cm and 2 cm.

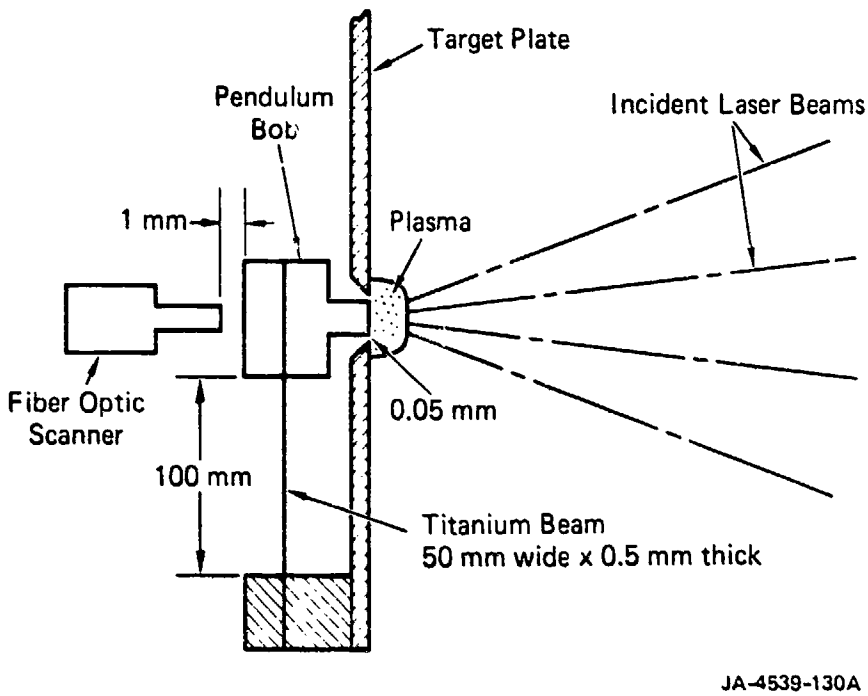

Figure 8. Pendulum used for impulse measurements.

SECTION 3

IN-AIR COUPLING EXPERIMENTS

The in-air experiments were performed at the Battelle Memorial Institute Columbus Laboratories. In these experiments Battelle used a neodymium-glass laser (1.06-μ wavelength) with a pulse energy ranging from 100 to 1000 J and a nominal pulse width of 30 ns (full width at half maximum). The experiments were performed with spot diameters of 1 or 2 cm.

The configuration of the Battelle laser uses four beams individually focused onto a single spot. The total energy incident on the target in each shot was determined by splitting a known fraction of the beam into a calorimeter. The temporal variation in flux was measured in each experiment by passing the beams through a beam splitter and measuring the fraction of the split beam with a photodiode. Figure 9 shows a typical photodiode record. Variations from shot to shot were minor.

The spatial variation in fluence was measured by Battelle with a film exposure technique. Light-sensitive film is exposed at a low fluence and scanned with an optical densitometer. Figure 10 shows horizontal and vertical scans for a 1-cm-diameter spot. It is assumed that the spatial and temporal distributions of fluence and flux are independent and vary proportionally with total pulse energy.

The measured spatial and temporal variations in flux and fluence determine the peak flux in the laser spot. The peak flux was found by dividing the total pulse energy by the area under the relative flux and fluence curves shown in Figures 9 and 10. This gives the peak flux as a function of pulse energy (E)

$$F = 2.7 \times 10^7 \frac{W/cm^2}{J} \times E$$

for a 1-cm-diameter spot and

$$F = 6.7 \times 10^6 \frac{W/cm^2}{J} \times E$$

for a 2-cm-diameter spot.

The average flux over the nominal pulse width of 30 ns (full width half maximum) is found by assuming a rectangular pulse with uniform fluence over the laser spot. In this case

$$F = 4.2 \times 10^7 \frac{W/cm^2}{J} \times E$$

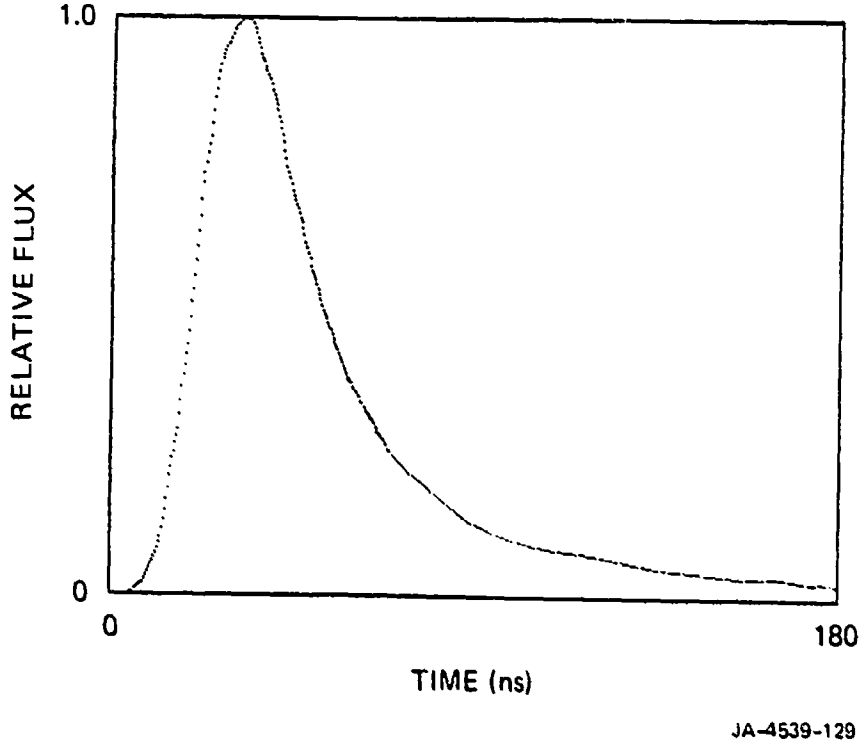

Figure 9. Relative flux measured with a photodiode.

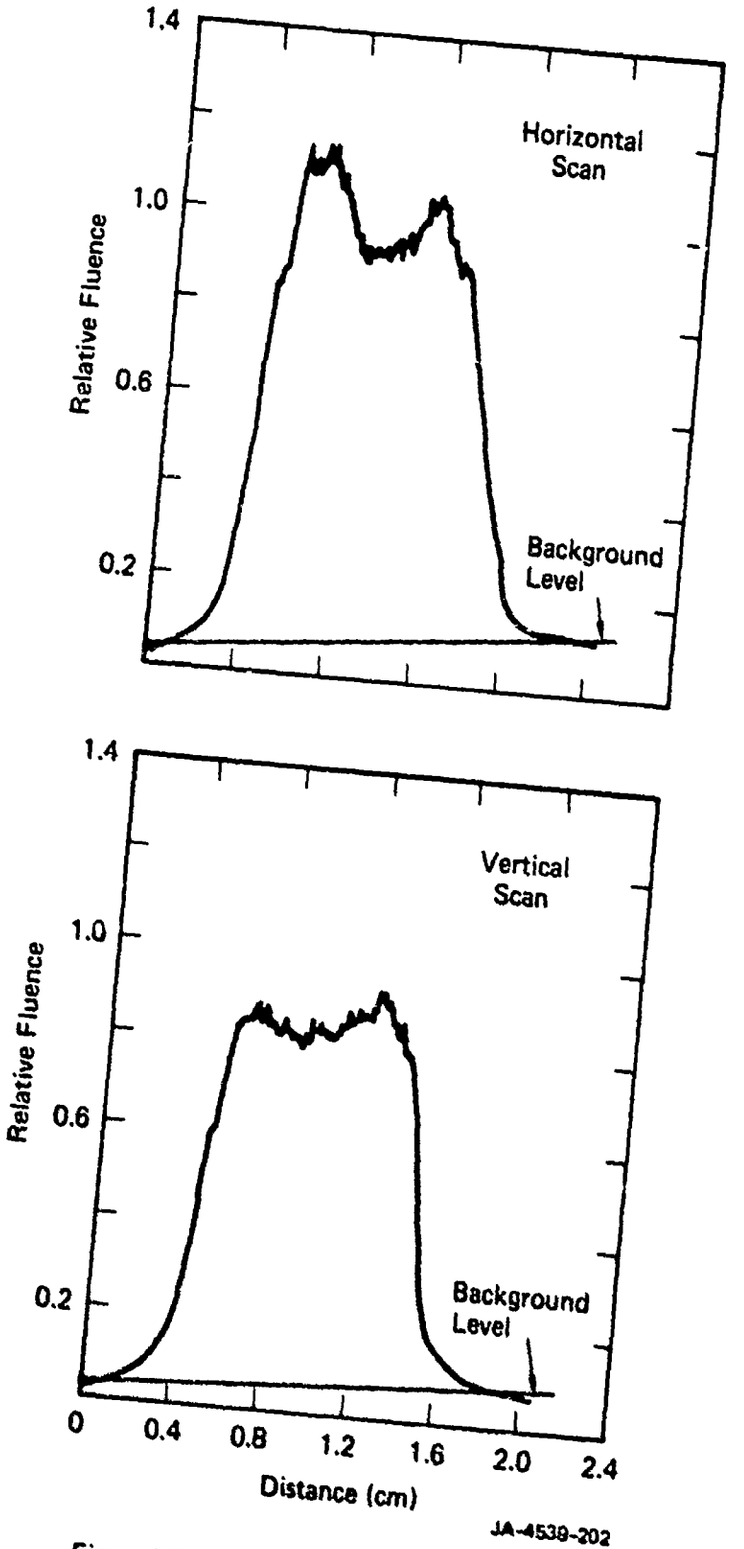

Figure 10. Spacial variations in fluence.

for a 1-cm-diameter spot. This larger value results because much of the laser energy is delivered over times much greater than 30 ns.

The laser coupling experiments at Battelle consisted of both pressure and impulse measurements*. Fourteen pressure histories were recorded (although more were attempted). All the pressure measurements were made at a spot diameter of 1 cm. Twenty-seven impulse measurements were made at spot diameters of 1, 2, 3, and 6 cm. Most of the impulse data were taken at pendulum diameters of 1 and 2 cm. The pressure and impulse data are summarized in Tables 2 and 3, respectively.

3.1 PRESSURE MEASUREMENTS.

Examples of pressure records taken at a 1-cm spot diameter (D) are shown in Figures 11 and 12. Figure 11 shows two pressure records taken under similar pulse energies and observed for relatively long times (5 μs, or more than 100 laser pulse widths). Both pressure records show similar behavior although they do not return to the baseline in the same way. The differences in late-time behavior are due to baseline drift caused by gage heating. As a consequence of this drift, there is an uncertainty in late-time pressures of ± 0.2 MPa (± 2 bar). The dip in indicated pressure between 2 and 3 μs is due to the three-dimensional stress effects on the gage that were discussed in the previous section. From the pressure records shown in Figure 11, we tentatively conclude that there is little surface overpressure after 5 μs and consequently little impulse accumulated after this time.

The four stress records shown in Figure 12 illustrate the variation in surface pressure with changing pulse energy. Each record has the same overall shape, but details in shape vary from shot to shot. From these data and shot-to-shot variations in the pressure records obtained at the same laser energy, the slight differences in these stress pressure records are probably due to variations in the mounting of the aluminum cover disk on the target surface. Although it is not clear at the time-scales shown, the rise time of the measured pressure pulse in some shots was between 30 and 40 ns. Of course, the actual rise time of the surface pressure

*As mentioned earlier, gage stress measurements are referred to as "pressure histories," but are actually measurements of the gage response just below the target surface.

Table 2. Summary of in-air pressure data obtained at 1 atm ambient pressure with a laser spot diameter (D) of 1 cm.

Shot	Target	Energy (J)	Peak Pressure (MPa)	Impulse Intensity[a] (Pa-s)[b]	Impulse (dyne-s)	t_1 (μs)	Peak Flux (10^9 W/cm^2)
6128	Al	203	93	54	420	2	5.5
6129	Al	197	89.5	47	370	5	5.3
6130	Al	197	102	53	420	2	5.3
6131	Al	197	102	53	420	2	5.3
6134	Al	472	186	89	700	2	12.7
6136	Al	91	61	32	250	2	2.5
6137	Al	91	61	32	250	2	2.5
6139	Al	200	100	53	420	2	5.4
6140	Al	200	88	40	310	2	5.4
6141	Al	353	148	71	560	2	9.5
6145	C	93	58	23	180	2	2.5
6146	C	71	190	97	760	5	2.5
6147	Al	900	210	105	820	2	24.3
6148	Al	879	240	161	1300	5	23.7

[a] Integral of pressure history from 0 to t_1 times spot area (0.785 cm^2)

[b] 1 Pa-s = 10 dyne-s/cm^2 = 10 taps.

Table 3. Summary of in-air impulse data obtained at 1 atm ambient pressure.

Shot	Target	Energy (J)	Spot Diameter (cm)	Pend. Diameter (cm)	Impulse (dyne-s)
6113	Al	771	1	1	1280
6114	Al	776	1	1	1310
6115	Al	843	1	1	1120
6150	Al	846	1	1	1120
6151	Al	812	1	1	1050
6152	C	780	1	1	1020
6118/08	Al	703	1	2	2548
6119/09	Al	744	1	2	2717
6120/10	Al	637	1	2	2470
6116	Al	424	1	1	690
6117	Al	329	1	1	645
6111	Al	380	1	2	1490
6112	Al	429	1	2	1670
6118	Al	169	1	1	421
6119	Al	209	1	1	482
6153	Al	182	1	1	497
6154	C	182	1	1	512
6156	Al	194	1	2	1085
6158	C	185	1	2	1038
6120	Al	66	1	1	209
6121	Al	97	1	1	297
4088	Al	808	2	3	3940
4089	Al	789	2	3	4080
4090	C	762	2	3	5060
4092	Al		2	3	3630
4095	Al	762	2	3	3930
4097	Al	841	2	6	9010

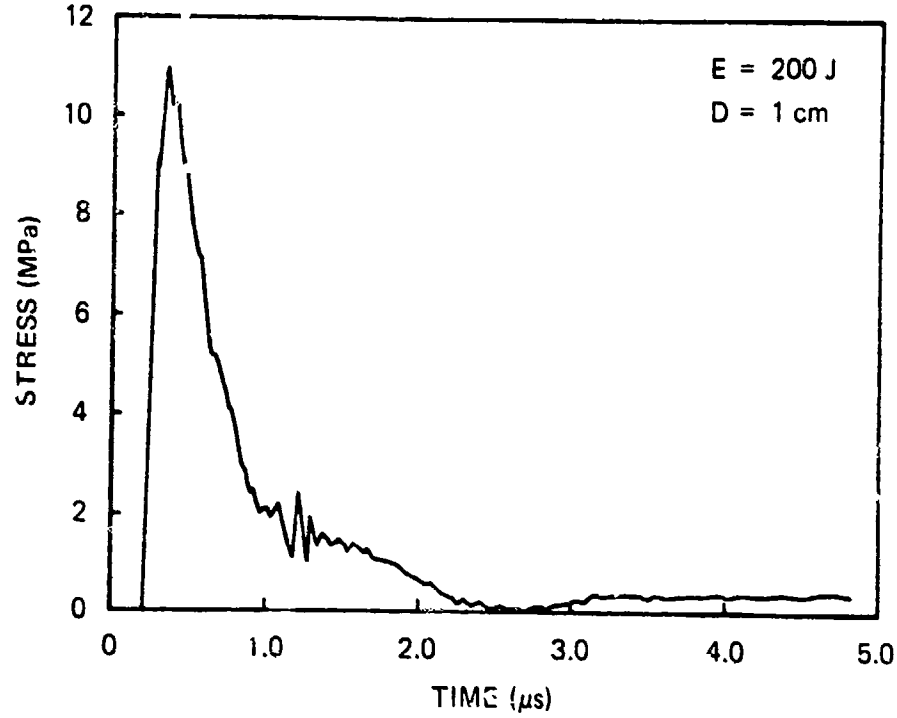

(a) Shot 6139

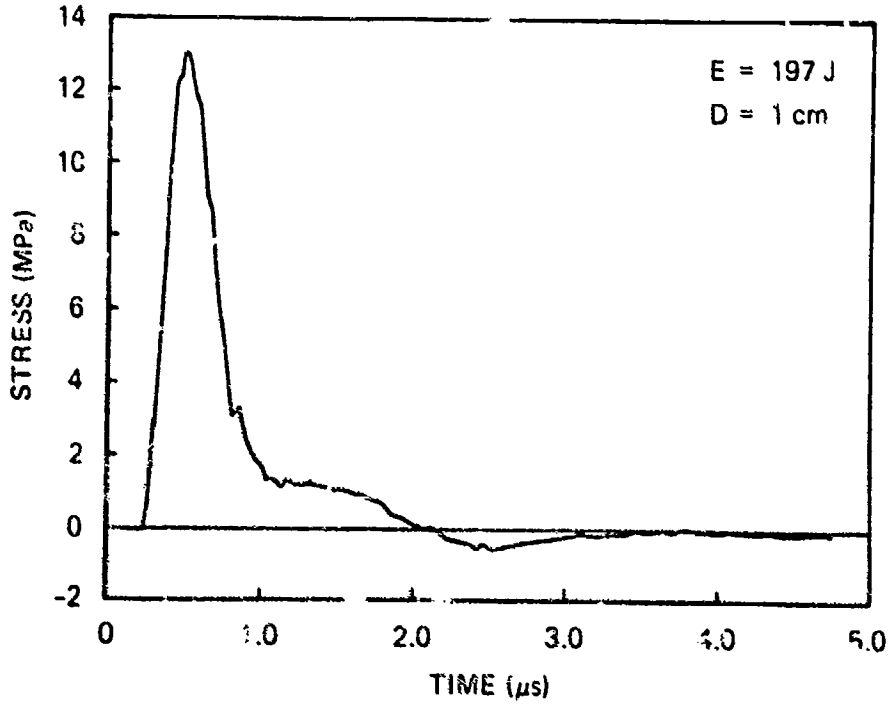

(b) Shot 6131

JA-4539-133A

Figure 11. Stress histories showing late-time response.

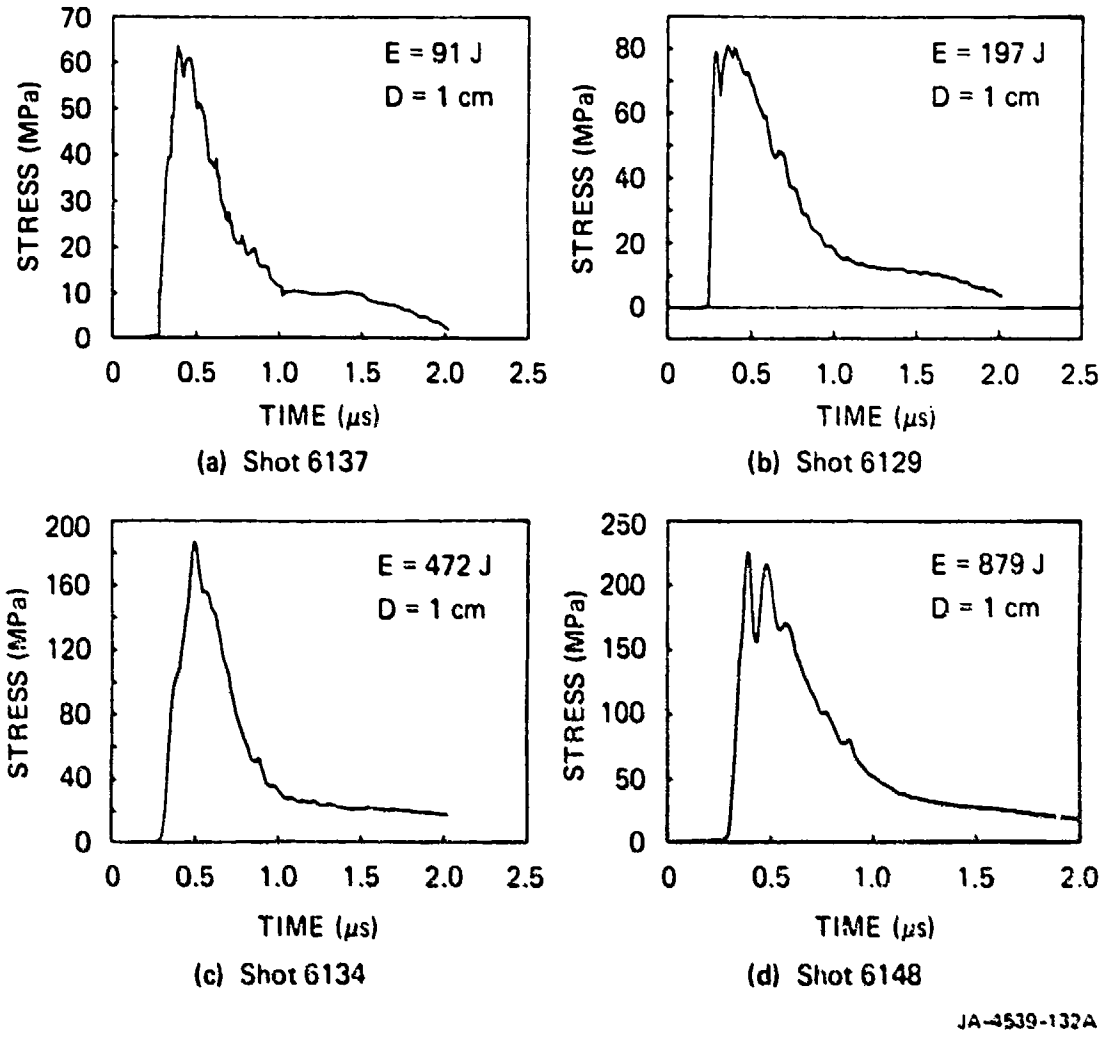

Figure 12. Stress-time histories recorded at different laser energies.

may be faster because the measured rise time is influenced by the layers in the gage package and any lack of simultaneity at the gage plane.

The peak surface pressures measured in these experiments are plotted as a function of the peak flux in Figure 13. These data show the general trend expected from current theories for laser-supported detonation (LSD) waves; that is, the peak pressure varies as the flux to the 2/3 power. However, the magnitude of the peak pressure is significantly below that predicted by the simple formulas derived in References 3-5. For comparison, a similar plot based on past data taken under different conditions (Reference 6) is also shown in Figure 13. The past data and analysis show significantly higher peak pressures. This difference has been attributed to the production of superdetonation (radiation-driven) absorption waves, and incorporation of a superdetonation model has given good agreement with the data (Reference 7). Additional support of the superdetonation hypothesis was the observation of higher-than-expected absorption wave velocities in other experiments performed during the test series at Battelle (Reference 7).

3.2 IMPULSE MEASUREMENTS.

The impulse data obtained using the 1- and 2-cm pendulums are plotted in Figure 14. These data show a strong dependence on pendulum diameter due to the effects of the blast wave produced by the laser plasma. Note that in two of the experiments, a graphite target was substituted for the aluminum target. This material substitution did not change the impulse.

The pendulum data can be compared with the impulse calculated by integrating the pressure gage records in space and time as a check on the contribution of late-time blast effect to impulse. The most meaningful comparison is for pendulum data obtained using the 1-cm pendulum and 1-cm diameter laser spot. In making this comparison, it is important to note that the pendulum area (1-cm-diameter circle) is larger than the area of the active element of the pressure gage (0.4-cm square); consequently, the spatial variation in impulse intensity (the impulse intensity is lower near the spot edge) will tend to lower the impulse measured by the pendulum with respect to impulse calculated from the gage data. At the same time, late-time blast effects will tend to make the pendulum reading higher than the integral of the pressure record (one of the effects we are looking for). As a result, our conclusions must be tentative. However, comparing the data in Tables 2 and 3 shows that the integral of the pressure histories is about 10 to 20% less than the impulse

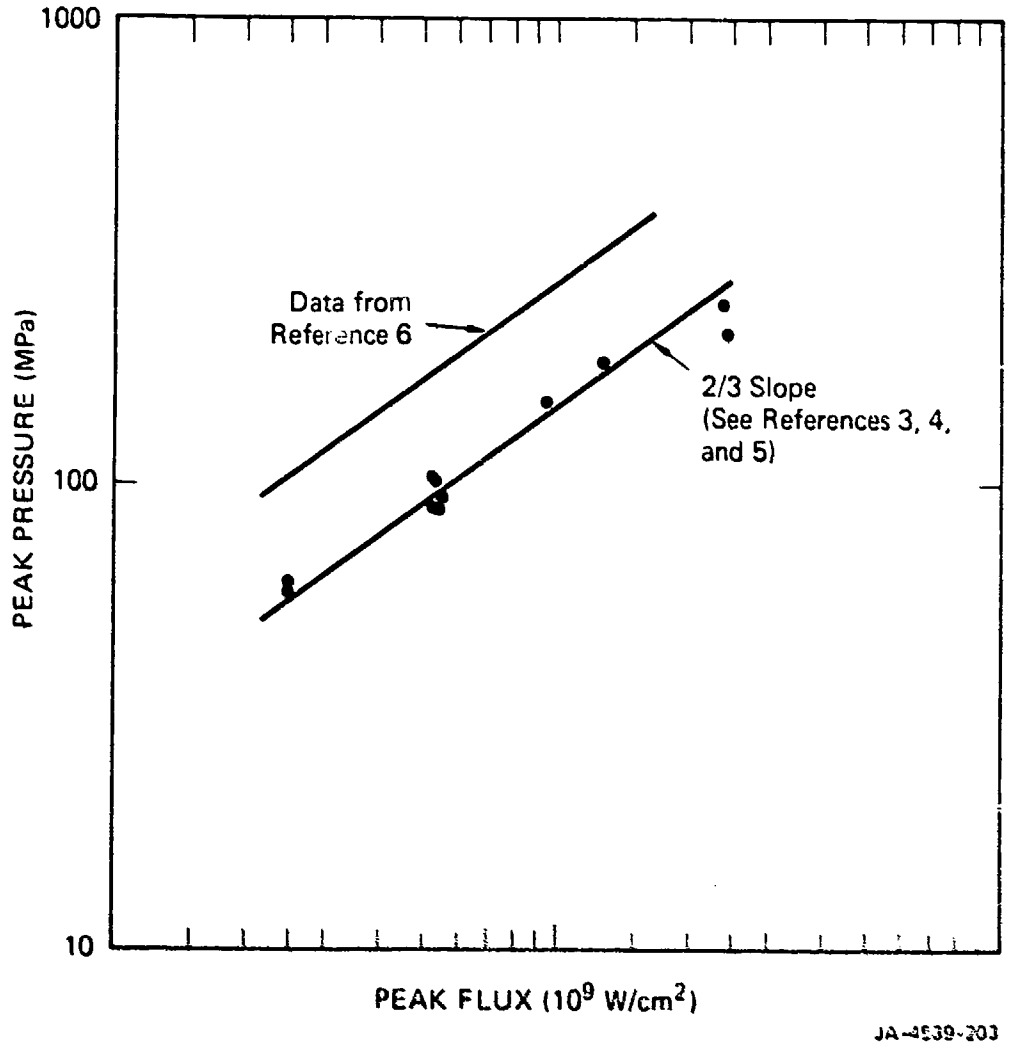

Figure 13. Peak pressure as a function of flux for aluminum targets. Expected relationship based on past theory and experiments is shown for comparison.

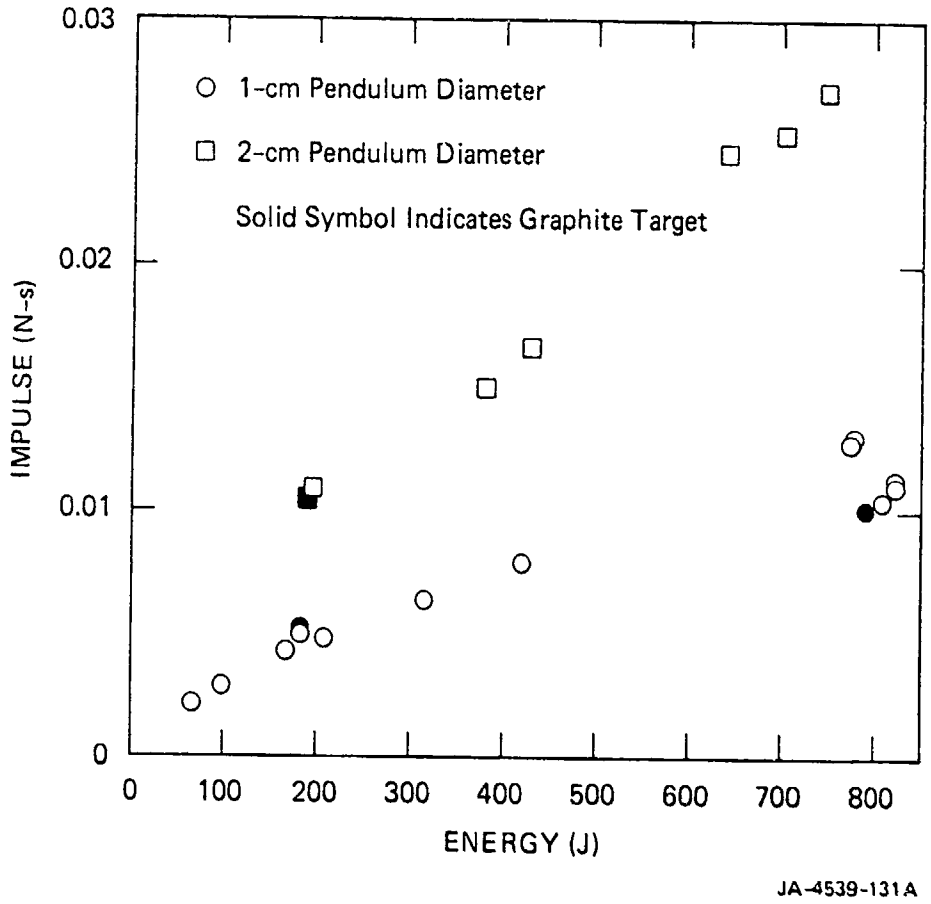

Figure 14. Impulse as a function of beam energy for 1-cm laser spot diameter.

intensities measured with the pendulum*. This indicates that the contribution of late-time impulse to total impulse is a least 10 to 20% of the total impulse.

Past experiments and analyses of in-air coupling can be used with the current data to obtain a better estimate of the the contribution of late-time impulse. In Reference 8, prompt impulse intensity was measured as a function of distance from the center of the laser spot. Within the laser spot and to a first approximation, impulse intensity varied inversely with spot radius so that

$$I = I_o (1 - Ar/R_o)$$

where I_o is the impulse intensity at the spot center, r is the radial coordinate, R is the spot radius, and A is a constant of proportionality and has values between 0.2 and 0.4.

Similar estimates were obtained for impulse intensity distribution through analysis in Reference 5 where it was shown that A depends on laser pulse duration. For pulse lengths approximately equal to the spot radius divided by the local sound speed in the plasma, A was found to be 0.4.

Assuming a value of A of 0.4, the impulse intensity measured by the gage (I_g) would be

$$I_g = \frac{2\pi \ I_o}{\pi \ R_g^2} \left[\frac{1}{2} (R_g)^2 + \frac{0.4}{3R} (R_g)^3 \right]$$

or for an effective gage radius of 2.4 mm:

$$I_g = 0.87 \ I_o$$

Similarly, the impulse intensity measured by the pendulum (I_p) is

$$I_p = 0.73 \ I_o$$

thus I_g/I_p should be 1.2 if there were no contribution from late-time impulse in the

*For example, for shots 6128-6131 (Table 2) the pressure gage data give an average impulse intensity of 52 Pa-s at an average pulse energy of 199 J; for shots 6118, 6119 and 6153 (Table 3) the pendulum data give us average impulse intensity measured over the pendulum of 59.4 Pa-s at an average pulse energy of 186 J.

pendulum measurement. Because I_g/I_p in the experiments was actually about 0.85, we conclude that the total contribution of late-time impulse within the total laser spot is about 40%. The implication is that pendulum measurements will tend to cause overestimates in structural damage unless a correction is made for pulse shape because the late-time impulse measured by the pendulum would not contribute to structural response.

The analysis of these experiments by S-Cubed (Reference 7) points to other effects that can alter late-time impulse. Specifically, it was found that the expansion of the plasma and air engulfed in the surrounding blast wave can produce a period of negative gage pressure that reduces the pendulum measurement of impulse. This period of reduced pressure would occur between 50 and 500 μs in the laboratory experiments according to the S-Cubed model of the expansion process. It would thus occur long after structural response is completed on full-scale targets, but it would still influence the results of the pendulum measurements described here. Examination of the calculations in Reference 7 shows that the reduction in measured impulse increases with the ratio of pendulum-to-spot diameter and decreases with increasing laser pulse energy. For the most common test conditions used (that is, spot diameters equal to the pendulum diameter and pulse energies greater than 100 J), the estimated effect on impulse was less than 5% and thus does not affect our previous calculation of prompt impulse.

Although the period of reduced pressure suggested by the analytical model proposed in Reference 7 had little effect in our experiments, we looked further for its influence in those experiments in which the pendulum diameter was larger than the laser spot diameter. In all the pendulum measurements, a continuous record was made of the displacement-time history from the beginning of the laser pulse to times as long as 5 μs. A typical record is shown in Figure 15 where the laser beam diameter was 1 cm and the pendulum diameter was 2 cm. Calculations in Reference 7 indicate that an offset of 20% might be expected for this record*. Because the slope of the displacement-time history at any time is the current total impulse, this record should show the effect anticipated in Reference 7 as an offset in the displacement-time history near the origin (between 0 and 0.2 ms). The amount of offset is proportional to the integral of the actual impulse to the current time minus the product of the average total impulse times the current time. The 20%

*Based on Figure 7.2.20 (R_p = 2 cm; E = 115 J) in Reference 7.

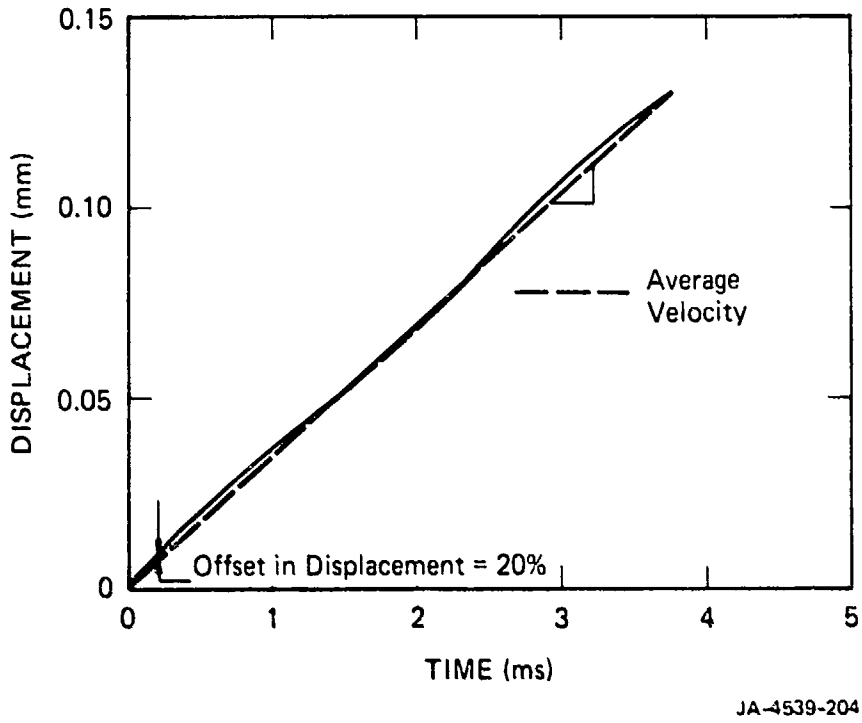

Figure 15. Pendulum displacement-time history for Shot 6156.

offset indicated in Figure 15 is difficult to measure from the record and may be due to other effects in the measurement. However, these records do not rule out the effect postulated in Reference 7 and suggest that more precise pendulum measurements may be able to detect it.

3.3 CONCLUSIONS FROM THE IN-AIR EXPERIMENTS.

The pressure measurement series for in-air coupling provides a self-consistent picture of in-air coupling. However, the pressure records do not fit well with past theories of laser-supported detonations because the measured peak pressures are too low. A further implication of the current measurements is that there is a significant contribution to total impulse from late-time effects. This means that impulse data obtained with pendulums should be used with caution when projecting weapons effects, and future impulse measurements should include some pressure history or impulse evolution measurements to correctly measure the prompt impulse.

SECTION 4

IN-VACUUM COUPLING MEASUREMENTS

Coupling measurements in a vacuum were obtained at the Scale-Up Laser Facility at Avco Everett Research Laboratory in Everett, Massachusetts. The Avco scale-up laser was operated using XeF as a lasing medium, resulting in primary wavelengths of 3.532 μm and 3.511 μm. For this experiment series the laser beam was directed through an aperture to give a circular spot (8 mm or 12.4 mm in diameter) of very uniform intensity and sharply defined edges. Targets were located in front of the focus of the beam, and spot diameter was adjusted by moving the target with respect to the focal point. Instrumentation for each shot included a measurement of the total beam energy and the temporal variation in flux. In separate experiments, Avco measured the spatial variation of fluence within the beam. Figure 16 is an example of the temporal variation of flux in the beam, and Figure 17 is an example of the spatial variation of fluence in the beam. As shown in Figure 16, the nominal pulse duration was 1.5 μs (full width at half maximum) in these experiments.

All the tests in this series were performed in a vacuum tank. For most of the tests, the pressure in the tank was about 5 torr for reasons that are explained later. Comparison of impulse data taken at 5 torr ambient pressure and data taken at less than 1 torr ambient pressure indicated that the coupling did not change over this range of pressure. In addition, examination of target surfaces also indicated that target damage did not change over this range of ambient pressures. However, at 5 torr, the burn patterns on aluminum targets did show a ring of soot that was not present at lower pressures. Figure 18 shows a burn pattern taken under these conditions. This pattern also illustrates the uniformity and circularity of the beam.

Seven data shots were performed in the in-vacuum test series. In addition, about ten shots were used to solve noise and other instrumentation problems, which were considerable. Some of these problems arose from the electrical and magnetic environment in the laser facility, but one additional problem was a result of the in-vacuum coupling process and the measurement electronics. This problem arises as an artifact of the coupling process and is illustrated in Figure 19. When the laser beam strikes and vaporizes the target surface, the plasma leaves the surface at high velocity. The lighter elements in the plasma, including electrons, move faster than the heavier elements, which include many positively charged ions. This "charge

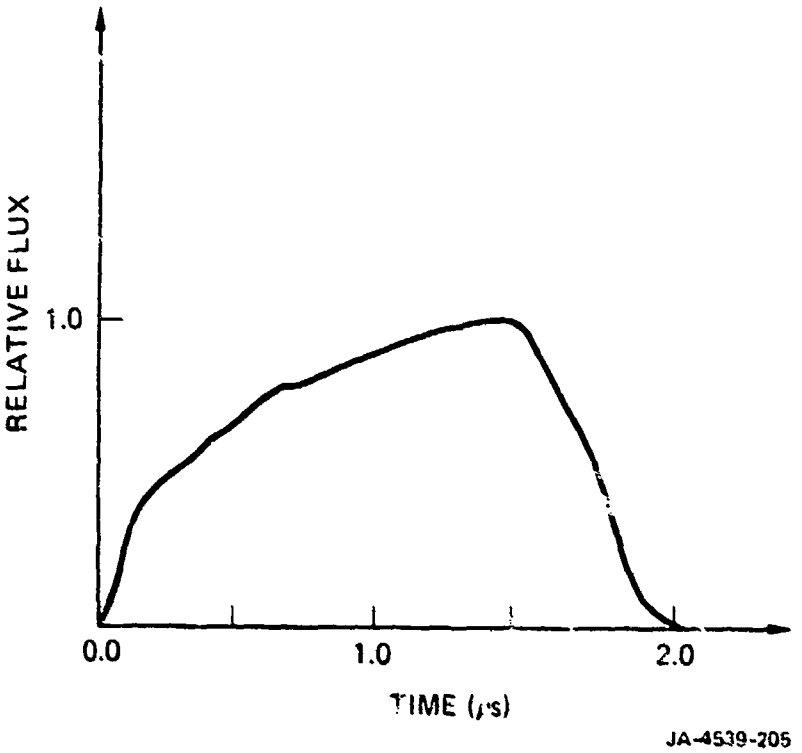

Figure 16. Pulse shape for scale-up laser.

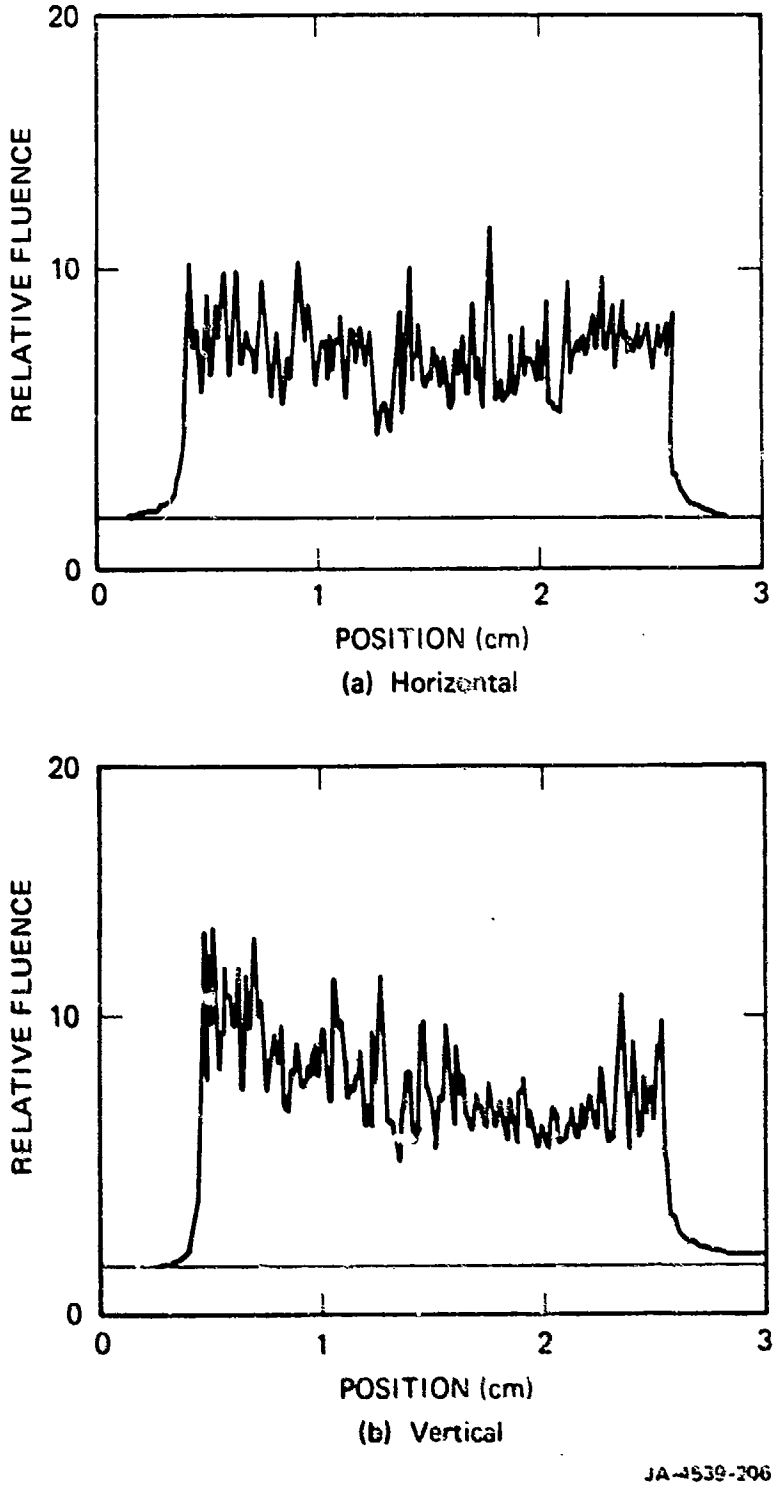

Figure 17. Spatial profile at target plane. Provided by Avco Everett Research Laboratory.

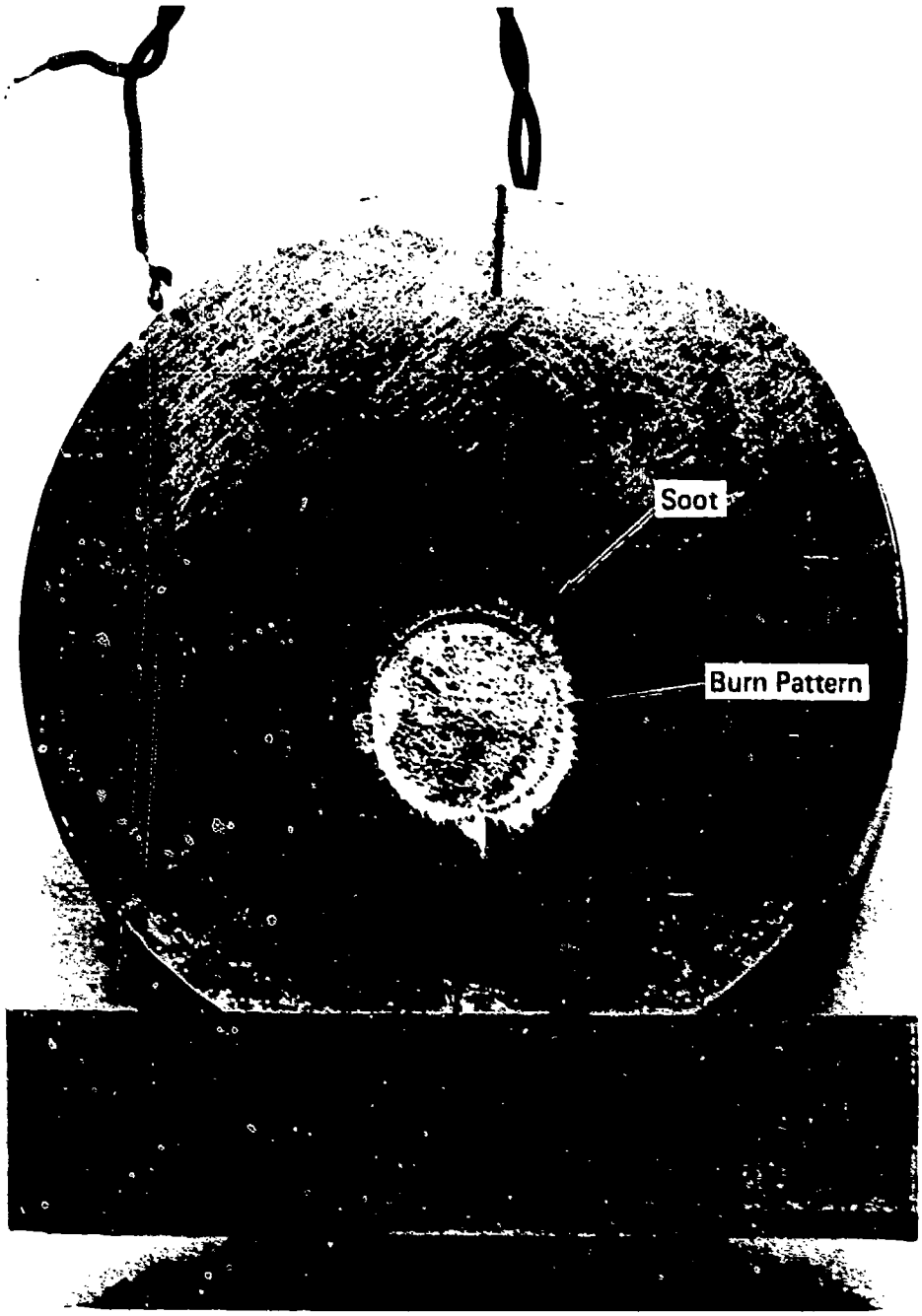

JP-4539-155

Figure 18. Burn pattern on gage package surface.

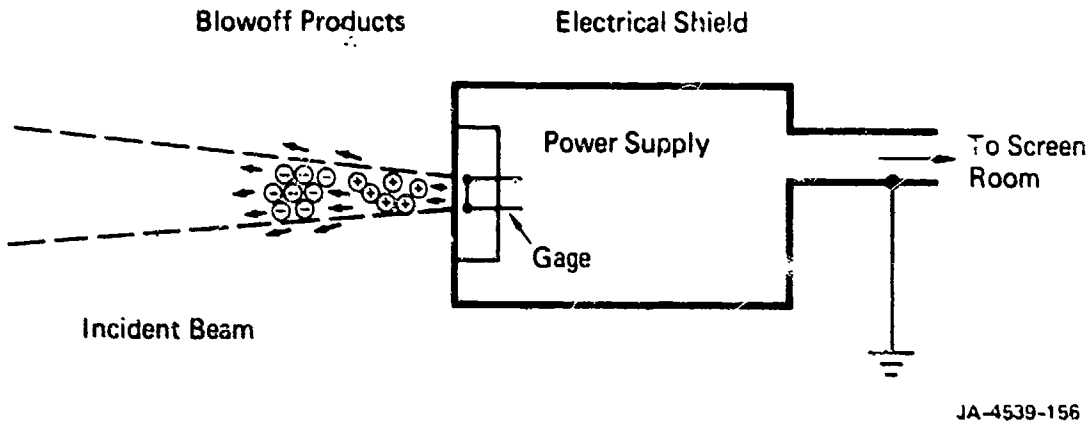

Figure 19. Charge separation problem.

separation" produces a strong electric field and charge in the target, and caused large shifts in the gage readings during some experiments.

Because of the time constraints in the experiments, we were unable to alter the electronics to offset the charge separation effect. However, we found that this effect could be eliminated by raising the pressure around the target to about 3 torr. Apparently, the small amount of air near the target was sufficient to eliminate the charge separation or provide a current path to short-circuit the charge.

An additional problem that was never fully eliminated was the presence of electromagnetic noise produced by the laser at the beginning and end of the laser pulse. This noise caused the pressure records to blur, as recorded on oscilloscope cameras. This blurring gave rise to some uncertainty in the pressure records from 0 to 0.5 μs and from 1.5 to 2.5 μs. Blurred portions of the pressure records shown below are indicated by a dashed line.

4.1 PRESSURE MEASUREMENTS.

The pressure data obtained in the Avco in-vacuum experiments are shown in Figures 20 through 23. The data shown in Figures 20 through 22 are for targets with aluminum cover plates, whereas the pressure record shown in Figure 23 is for an aluminum cover plate with a 0.25-mm coating of Epon 828 epoxy. Examination of the pressure records shows that in the case of the aluminum targets, the pressure history has a shape similar to the incident laser pulse. In all the experiments there was some ambiguity in the pressure record after the laser pulse stopped, due to electrical noise from the laser. This region usually occurs between 1.5 and 2.5 μs. In those records where the pressure trace was lost, no indication of pressure history is given. In those records where the pressure history was recorded but showed significant noise, the average of the noisy signal is indicated by a dashed line. Some pressure records also showed noise at the beginning of the trace as indicated by a dashed line at early times.

The pressure record obtained using the epoxy coated target (Figure 23) has a much different appearance from the records obtained using uncoated aluminum targets. In this experiment, the pressure history was characterized by a step, followed by a long decay. This type of pressure history is characteristic of an LSD plasma ignition. Examination of the target after the experiment showed that all the epoxy in the laser spot was removed during the experiment, either through shock or

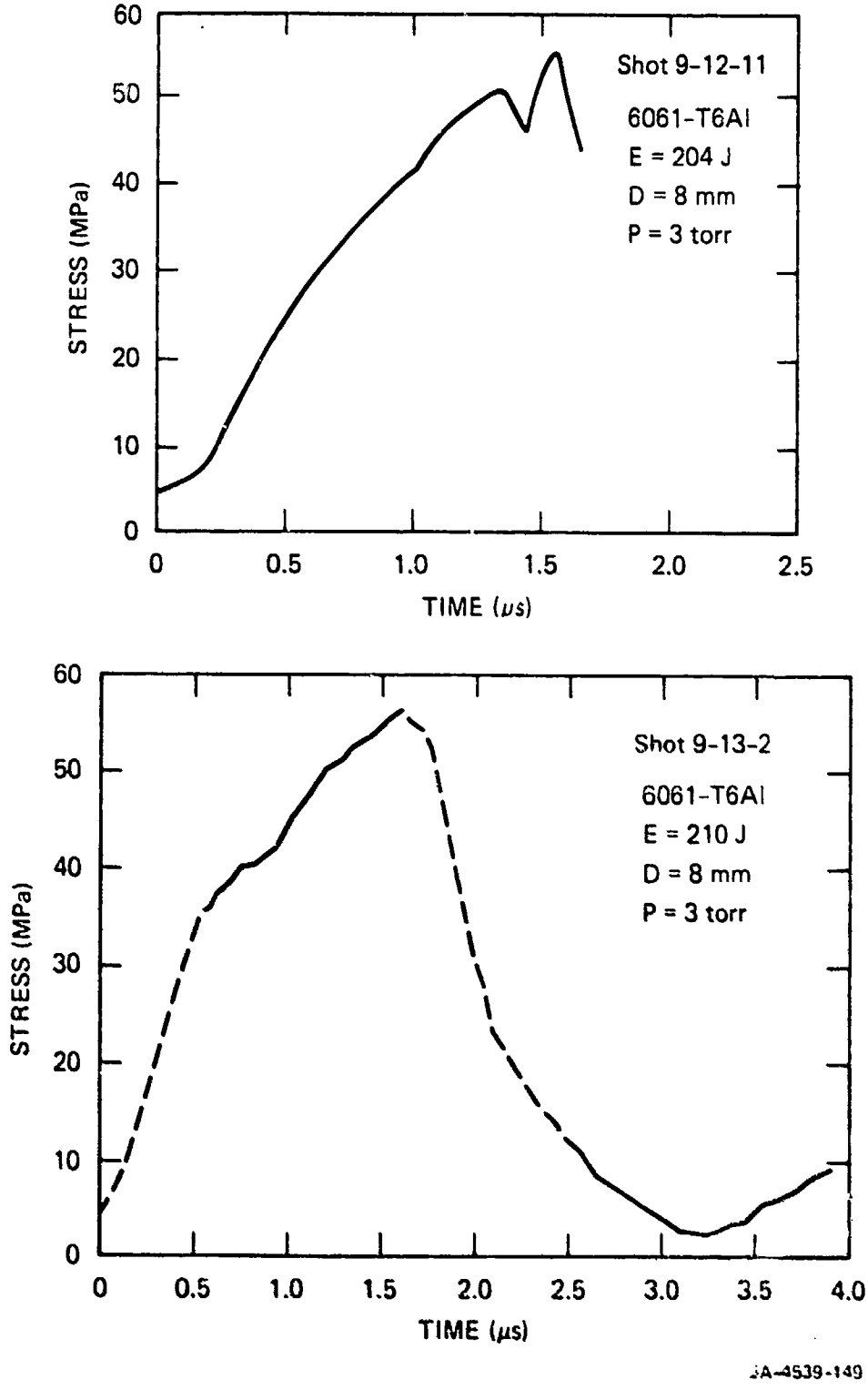

Figure 20. Stress-time history for Shots 9-12-11 and 9-13-2. (Dashed lines represent blurred portions of the pressure records.)

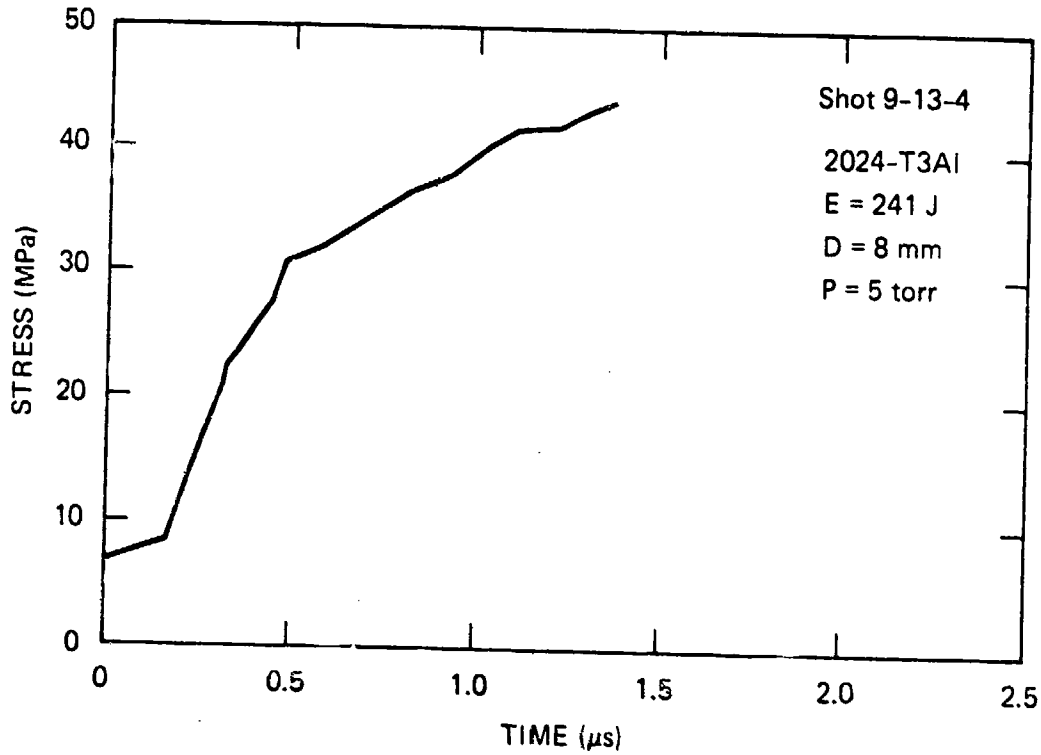

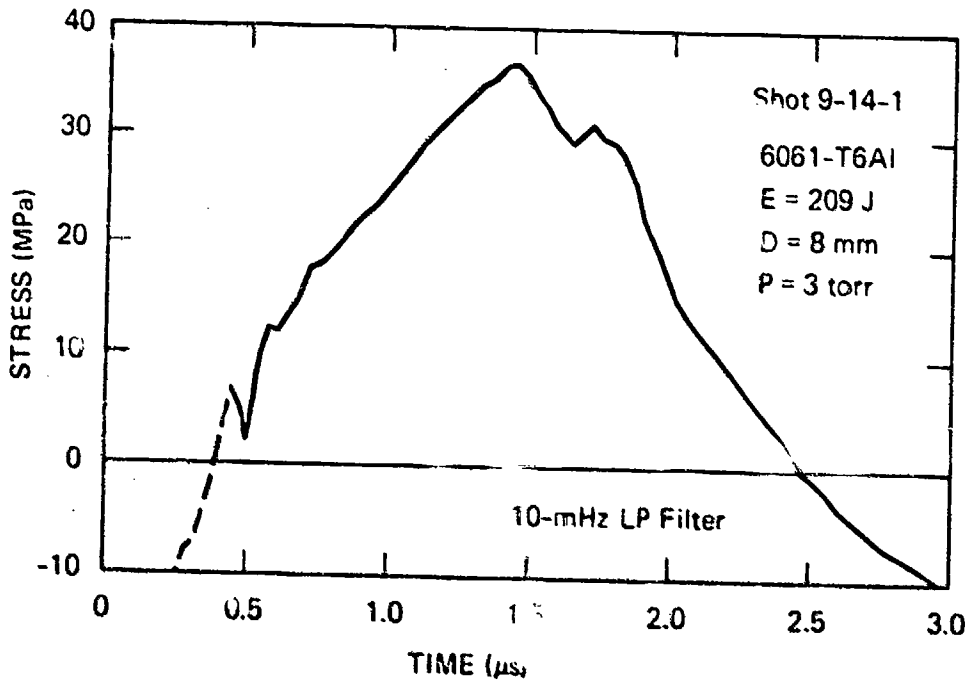

JA-4539-150

Figure 21. Stress-time history for Shots 9-13-4 and 9-14-1. (Dashed line represents blurred portion of the pressure record.)

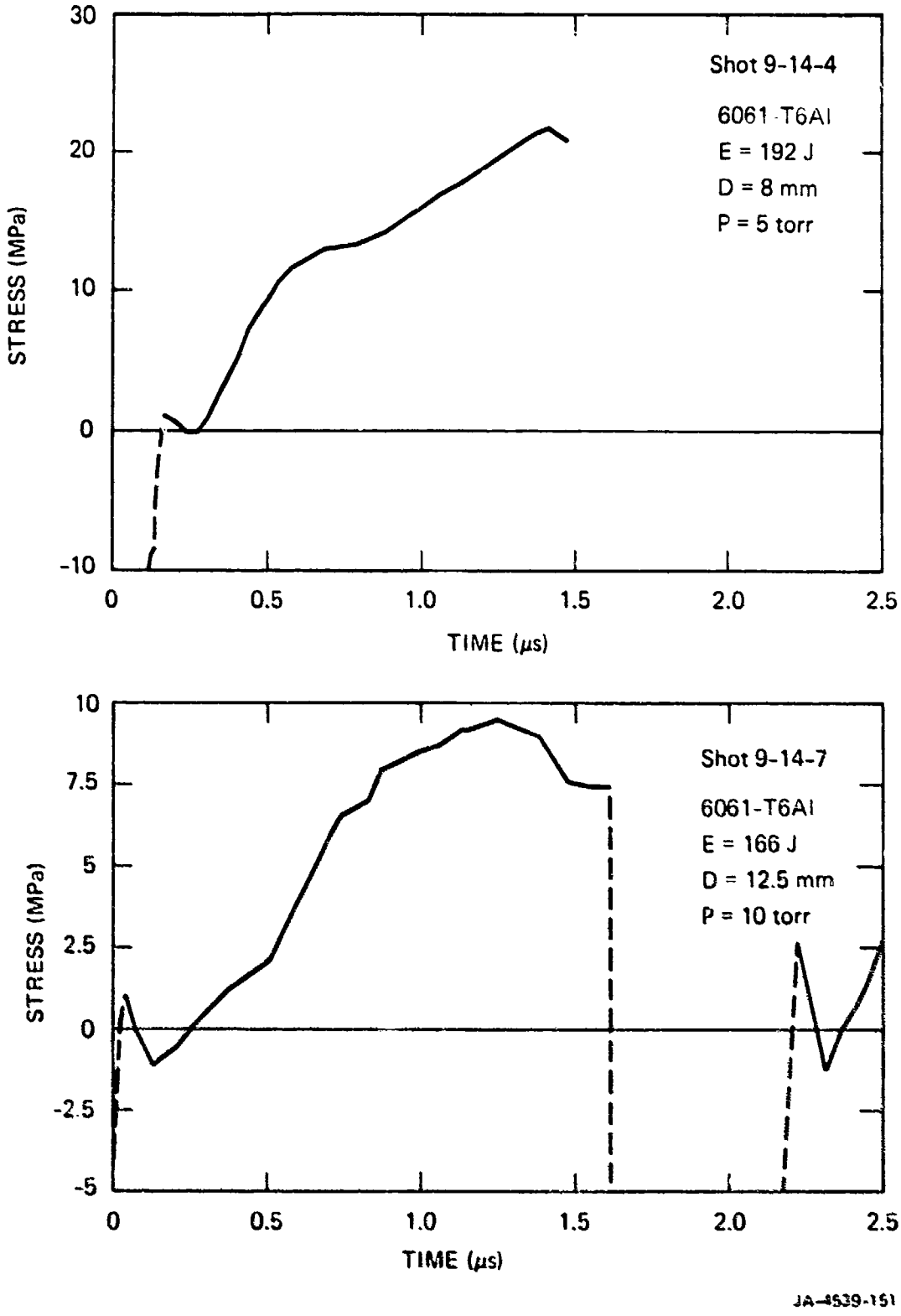

Figure 22. Stress-time history for Shots 9-14-4 and 9-14-7. (Dashed lines represent blurred portions of the pressure records.)

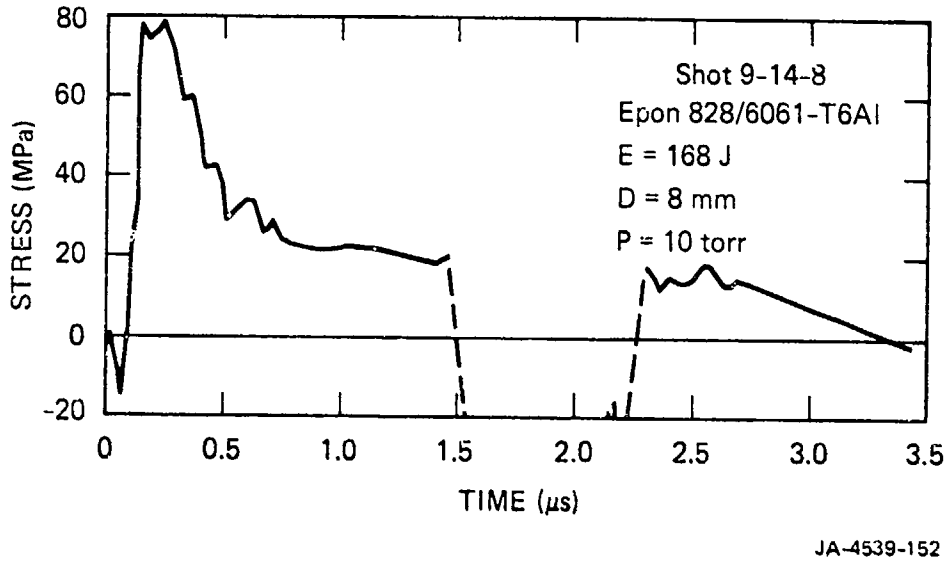

Figure 23. Stress-time history for Shot 9-14-8 using epoxy-coated 6061-T6 aluminum. (Dashed lines represent blurred portions of the pressure records.)

thermal damage. Based on the pressure record taken during the experiment, it appears that the laser pulse vaporized more of the epoxy layer in this experiment than it did aluminum in the bare aluminum experiments. This blowoff formed an absorbing plasma that mimiced the LSD wave response recorded in the in-air experiments.

The data from the Avco in vacuum experiments are given in Table 4. Peak fluxes shown in the data were calculated from the spatially averaged recorded flux and the nominal spot area based on the spot diameter listed in the table. Impulse intensities in the table were calculated from the areas under the pressure-time history curves from time zero or the first positive pressure indication to the time the trace ends or becomes blurred (a dashed line in the figures). Thus, the impulse intensity values are not evaluated over a constant time interval because of the varied durations of the pressure-time-history data.

Figures 24 and 25 show peak pressure as a function of peak flux and impulse intensity as a function of pulse energy, respectively. Both figures show a good deal of scatter, especially the impulse-intensity data. The peak pressure data (Figure 24) indicate that peak pressure increases by about a factor of 5 when the laser flux is increased by about a factor of 3. The impulse-intensity data indicate a similar strong sensitivity to pulse energy. These trends are difficult to determine more accurately because of the limited range of fluxes and energies accessible during the experiments.

4.2 CONCLUSIONS FROM THE IN-VACUUM EXPERIMENTS.

The data from the in-vacuum coupling experiments show the general characteristics expected of coupling due to target vaporization. With the exception of the epoxy-coated aluminum target, the pressure histories measured in the experiments have the shape of the incident laser flux history, indicating that the rate of mass removal and blowoff velocity, and hence surface pressure, vary directly with incident flux. Peak pressures measured in the experiments also vary with incident flux but show significant scatter. Peak pressures show a sharp increase with increasing flux at fluxes above 10^6 W/cm^2.

Because of the difficulties experienced with electromagnetic noise during the experiments, the impulse intensities found by integrating the pressure-time histories also show significant scatter. Impulse intensities increase sharply with increasing fluence at fluences of about 400 J/cm. Coupling coefficients found by integrating the pressure-time histories ranged from 0.25 to 1.5 dyne-s/J.

Table 4. Summary of data from the in-vacuum experiments.

Shot	Target	Energy (J)	Spot Diameter (mm)	Peak Flux W/cm^2	Peak Pressure (bar)	Impulse Intensity (taps)
9-12-11	Al	204	8.0	3.2×10^8	550	590
9-13-2	Al	210	8.0	3.3×10^8	560	500
9-13-4	Al	241	8.0	3.8×10^8	440	340
9-14-1	Al	209	8.0	3.3×10^8	380	360
9-14-4	Al	192	8.0	3.0×10^8	210	110
9-14-7	Al	166	12.5	1.1×10^8	93	85
9-14-8	Epoxy/Al	168	8.0	2.7×10^8	800	450

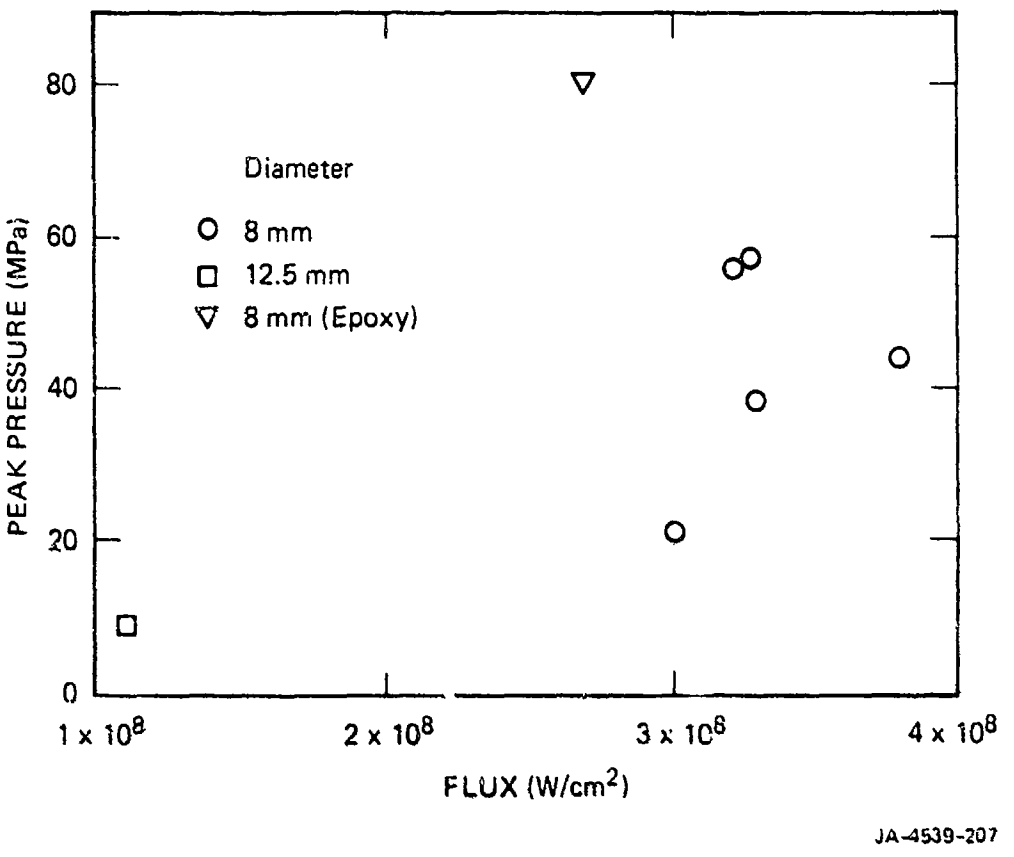

Figure 24. Peak pressure as a function of flux.

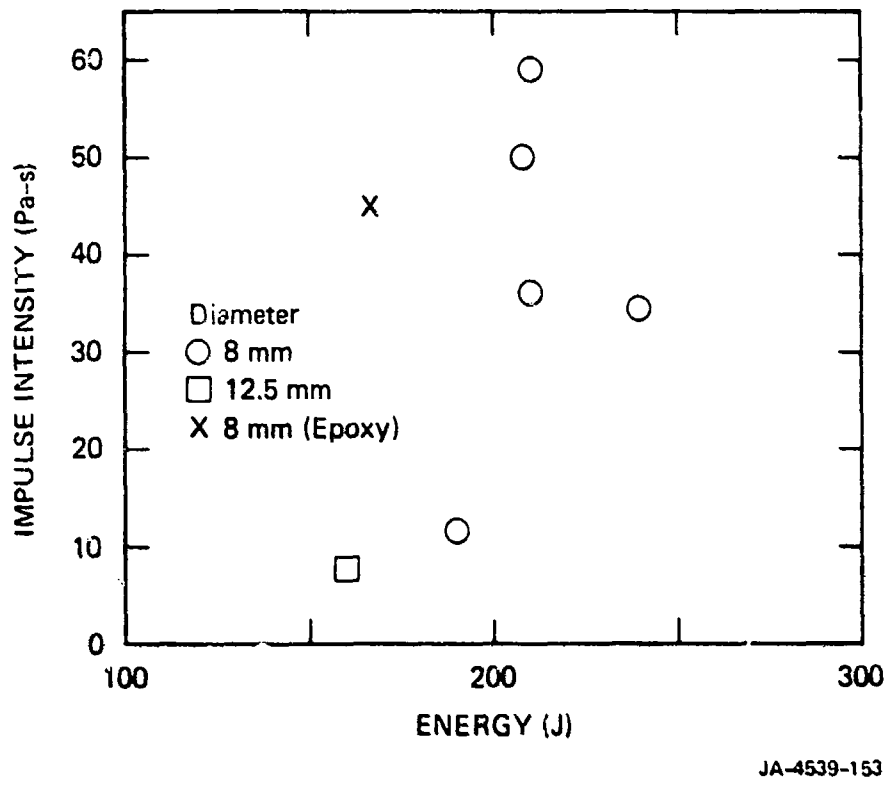

Figure 25. Impulse intensity as a function of laser energy.

SECTION 5

LIST OF REFERENCES

1. G. Weyl, A. Pirri, and R. Root, "Laser Ignition of Plasma Off Aluminum Surfaces," AIAAJ. 19(4), 460-469 (April 1981).

2. B. S. Holmes and J. D. Colton, "Application of Scale Modeling Techniques to Crashworthiness Research," in Aircraft Crashworthiness, edited by K. Saczalski et al. (University Press of Virginia, Charlottesville, VA, 1958).

3. A. N. Pirri, "Theory for Momentum Transfer to a Surface with a High Power Laser," Phys. of Fluids, 15(9), 1435-1440 (September 1973).

4. Y. P. Raizer, "Heating of a Gas by a Powerful Light Pulse," Soviet Phys. Jetp, 21(5), 1009-1017 (November 1965).

5. B. S. Holmes, C. Tarver, D. Erlich, and H. E. Lindberg, "The Mechanical Loads from LSD Waves and Their Simulation, Vol. I, Analysis and Pressure Measurements," SRI International (March 1976).

6. B. S. Holmes, W. E. Mayer, and R. B. Hall, "Laser Target Interaction Near the Plasma Formation Threshold," J. Appl. Phys., 51(11), 5699-5707 (November 1980).

7. M. H. Pice, J. R. Triplett, and G. A. Gurtman, "Analysis of 10.6 and 1.06 Laser Supported Detonation Wave Experiments," S-Cubed Final Report (April 1985).

8. B. S. Holmes and D. C. Erlich, "Surface Pressures from Laser Supported Detonations," J. Appl. Phys., 48(6) 2396-2403, (June 1977).

DISTRIBUTION LIST

DEPARTMENT OF DEFENSE

DEF RSCH & ENGRG
ATTN: ENGR TECH J PERSCH

DEFENSE ADVANCED RSCH PROJ AGENCY
ATTN: F PATTEN

DEFENSE INTELLIGENCE AGENCY
ATTN: RTS-2B

DEFENSE NUCLEAR AGENCY
ATTN: SPLH
ATTN: SPWE
4 CYS ATTN: TITL

DEFENSE TECHNICAL INFORMATION CENTER
12 CYS ATTN: DD

STRATEGIC DEFENSE INITIATIVE ORGANIZATION
ATTN: T/SL P TERRY

DEPARTMENT OF THE ARMY

U S ARMY MATERIAL TECHNOLOGY LABORATORY
ATTN: R FITZPATRICK

U S ARMY MISSILE COMMAND
ATTN: AMSMI-RD-UB H GREENE

U S ARMY STRATEGIC DEFENSE COMMAND
ATTN: SDC/S BROCKWAY

DEPARTMENT OF THE NAVY

NAVAL INTELLIGENCE SUPPORT CTR
ATTN: NISC-11 A COBLEIGH

NAVAL POSTGRADUATE SCHOOL
ATTN: PROF K E WOEHLER, CODE 61WH

NAVAL RESEARCH LABORATORY
ATTN: CODE 4600 D NAGEL

NAVAL SEA SYSTEMS COMMAND
2 CYS ATTN: PMS
ATTN: R RUDKIN

NAVAL SURFACE WEAPONS CENTER
ATTN: CODE R-31 J THOMPSON

OFFICE OF NAVAL TECHNOLOGY
ATTN: CODE 217

STRATEGIC SYSTEMS PROGRAM OFFICE (PM-1)
ATTN: NSP-L63 (TECH LIB)

DEPARTMENT OF THE AIR FORCE

AIR FORCE CTR FOR STUDIES & ANALYSIS
ATTN: AFCSA/SAMI (R GRIFFIN)

AIR FORCE SYSTEMS COMMAND
ATTN: DLWM

AIR FORCE WEAPONS LABORATORY, NTAAB
ATTN: TALE T EDWARDS

AIR FORCE WRIGHT AERONAUTICAL LAB
ATTN: MLPJ/DR S R LYON

FOREIGN TECHNOLOGY DIVISION, AFSC
ATTN: A CORDOVA

DEPARTMENT OF ENERGY

EG&G IDAHO INC
ATTN: J EPSTEIN

LAWRENCE LIVERMORE NATIONAL LAB
ATTN: F SERDUKE
ATTN: L-84 H KRUGER
ATTN: M GERRISSIMENRO

LOS ALAMOS NATIONAL LABORATORY
ATTN: B259 MS A GREENE
ATTN: C931 MS T KING
ATTN: E548 R S DINGUS
ATTN: J PORTER

SANDIA NATIONAL LABORATORIES
ATTN: M BIRNBAUM

SANDIA NATIONAL LABORATORIES
ATTN: DR J POWELL
ATTN: K MATZEN

DEPARTMENT OF DEFENSE CONTRACTORS

AEROSPACE CORP
ATTN: H BLAES

APTEK, INC
ATTN: DR E FITZGERALD

HAROLD ROSENBAUM ASSOCIATES, INC
ATTN: G WEBER

JAYCOR
ATTN: M TREADAWAY

KAMAN SCIENCES CORP
ATTN: J CARPENTER
ATTN: R ALMASSY

KAMAN TEMPO
ATTN: DASIAC

KAMAN TEMPO
2 CYS ATTN: DASIAC

KTECH CORP
ATTN: D KELLER

MCDONNELL DOUGLAS CORP
ATTN: L COHEN

PACIFIC-SIERRA RESEARCH CORP
ATTN: H BRODE, CHAIRMAN SAGE

PHYSICAL SCIENCES, INC
ATTN: A PIRRI

PHYSICS INTERNATIONAL CO
ATTN: M KRISHNAN

R & D ASSOCIATES
ATTN: B GOULD
ATTN: D GAKENHEIMER
ATTN: F A FIELD

S-CUBED
ATTN: G GURTMAN

SCIENCE APPLICATIONS INTL CORP
ATTN: H JANEE

SRI INTERNATIONAL
2 CYS ATTN: B HOLMES
ATTN: D CURRAN

W J SCHAFER ASSOCIATES, INC
ATTN: J REILLY